UNIVERSITY OF CALIFORNIA

Santa Barbara

Investigation of Anisotropic Thermal Conductivity of GaAs/AlAs Superlattices

A thesis submitted in partial satisfaction of the

requirements for the degree Master of Science in Electrical and Computer Engineering

by

Ran Li

Committee in charge:

Professor John Bowers, Chair

Professor Chris Palmstrom

Professor Jon Schuller

Dr. Ashok Ramu

September 2016

The thesis of Ran Li is approved.

____

Chris Palmstrom

____

Jon Schuller

____

Ashok Ramu

____

John Bowers, Committee Chair

September 2016

Investigation of Anisotropic Thermal Conductivity of GaAs/AlAs Superlattices

Copyright © 2016

by

Ran Li

ACKNOWLEDGEMENTS

First, I would like to thank my advisor, Professor John Bowers, for giving me the opportunity to conduct research in Optoelectronics Research Group and for giving me the guidance to finish my master's thesis. He is nice, supportive, and truly cares about his students! It is my honor and luck to be able to work in his group this year!

I also want to thank Dr. Ashok Ramu for giving me the opportunity to conduct this specific research! I am thankful for all his teachings and guidance while conducting my research and for his help examining and revising the content of my thesis!

Thank you to Professor Chris Palmstrom and Professor Jon Schuller for being the committee members in my committee and for their great teachings during my study here! Professor Palmstrom is such a nice and patient teacher! Likewise, Professor Schuller is a great teacher in his quantum physics class, where I learned a great deal of knowledge!

Thank you to Nicole Halaszynski for her patience in teaching me how to use the equipment and how to set up my experiments in the Thermoelectrics lab.

Thank you to Jon Peter and Justin Norman for helping me with the fabrications and measurements of my samples and for explaining the fabrication details of the silicon dioxide and superlattices.

Thank you to Jacie Valentine for her patience, support, and hard work in revising my entire thesis!

Thank you to all the people I met in the Thermoelectrics Lab and Optoelectronics Research Group for all their help and interesting conversations! Thank you to all the teachers, classmates, and friends from the University of California, Santa Barbara for their great teachings and help!

I also want to thank all my teachers, classmates, and friends from the University of Illinois, Urbana-Champaign for their instructions and support! Especially, I want to thank my first teacher in the solid-state electronics and materials area, Mohamed Mohamed from the University of Illinois, Urbana-Champaign! A big thanks for his encouragements and help on my journey of learning electronics!

Thank you to IFL in Champaign and ISI in Santa Barbara for giving me a family when I was alone in the United States. They are some of my greatest memories and gains in the U.S.!

Especially, I want to express my largest gratitude to my parents, Mingxia Sun and Chenghe Li, and my elder brother, Dawei Li! Thank you for your love, care, and company while I grew up! Thank you to my fiancé Xu Qian: Although you have been in China physically, you have given me unconditional love and support every day throughout these two years at UCSB! I want to send an extra thank you to you!

Thank you to all the angels that God sent to me! Thank you to all the friends who helped and encouraged me!

ABSTRACT

Investigation of Anisotropic Thermal Conductivity of GaAs/AlAs Superlattices

by

Ran Li

The thermal conductivities of superlattices are essential to improve the properties of thermoelectrics and optoelectronics; however, limited results in relation to both the in-plane and cross-plane thermal conductivities have been reported. A convenient, effective, and accurate experimental method is required to improve the current research on the thermal properties of superlattices. We conducted an experimental research study on two GaAs/AlAs superlattice samples with a total superlattice layer thickness of 2 μm using a combination of the 2-omega and 3-omega techniques. The samples have period thicknesses of 4 nm and 10 nm, respectively.

To explore the thermal conductivities of the substrate and insulation layer of the superlattice samples indirectly, a controlled sample with the same structure, but without a superlattice layer, is used. We obtained the thermal conductivities of the GaAs substrate and insulation layer (SiO_2 thin film) using the 3-omega technique and FEM simulation model. We also explored the deviation of the experimental results of the 2-omega technique from the Fourier's Law through the controlled sample. These parameters obtained from the controlled sample are used in the data analysis in the following superlattice research. In the superlattice study, we combine the 3-omega and 2-omega techniques to characterize the anisotropic thermal conductivity of GaAs/AlAs superlattice from the same wafer. The in-plane thermal conductivity, cross-plane

thermal conductivity, and anisotropy are obtained from the same wafer by comparing the experimental results with the FEM simulated results. This combination works fine in general and demonstrates a significant reduction in thermal conductivity compared to that of equivalent bulk materials. Superlattices with different period thicknesses but the same total superlattice thickness present a significant difference in both the in-plane and cross-plane thermal conductivities of the superlattices. However, we have found that the 3-omega technique is sensitive to the thermal conductivity of the insulation layer, which will affect the reliability of the results if the measured SiO_2 thermal conductivity is not accurate enough.

However, this effect should be able to be reduced or eliminated by using a much wider metal line than that used in the current research, and the reason for this is explained in the future work section of the last chapter. In addition, the numerical simulation results of the different thicknesses and different anisotropies of superlattices by considering the minimum and maximum SiO_2 thermal conductivities are also presented in the last chapter for future reference. The thermal conductivity variance in SiO_2 has a small effect in general, particularly on the 2 µm and 10 µm thick superlattices when a 10 µm wide wire is used in the 3-omega FEM model.

TABLE OF CONTENTS

ACKNOWLEDGEMENTS iv

ABSTRACT vi

TABLE OF CONTENTS viii

LIST OF FIGURES xi

Chapter 1 Introduction 1

1.1The purpose of this chapter 1

1.2 Background – meaning, challenge of superlattice thermal conductivity study, and our research 1

1.2.1 Applications of the superlattice 2

1.2.2 The challenge of superlattice thermal conductivity research 3

1.2.3 Our research 4

1.3 Techniques for measuring the anisotropic thermal conductivity of the superlattice and their results in recent research 5

1.3.1 3-omega method and two-varying-wire 3-omega method 5

1.3.2 AC calorimetric method 8

1.3.3 Optical pump-and-probe method (or time-domain thermoreflectance [TDTR]), transient thermal grating method (TTG), and their combination 10

1.3.4 Summary of the literature review 14

1.4 Overview of this thesis 15

Chapter 2 Theory of the 3-omega Technique and the Idea of the 2-omega Technique16

2.1 The goal of this chapter 16

2.2 The 3-omega method 16
2.2.1 3-omega method for substrate thermal conductivity 16
2.2.2 The 3-omega method to extract the isotropic thin film thermal conductivity and the FEM simulation model 23
2.3 The simulation prediction and the idea of the 2-omega method for anisotropic thin film 25
2.4 Summary and conclusion 28
Chapter 3 Experimental Methodology 29
3.1 The purpose of this chapter 29
3.2 The sample preparation 29
3.2.1 The controlled sample 29
3.2.2 Superlattice samples 30
3.3 Experimental setups and procedures 32
3.3.1 The experimental setup of the 3-omega technique on the controlled sample 33
3.3.2 The 2-omega technique experimental methodology on the controlled sample 35
3.3.3 3-omega and 2-omega set-ups for the two superlattice samples 37
3.3.4 Other parameters: Real dimensions of the devices and TCR of the metal line 38
3.4 Summary and conclusions 40
Chapter 4 Data Analysis, Experimental Results, and Discussion 41
4.1 The purpose of this chapter 41
4.2 Controlled sample 42

4.2.1 The thermal conductivity of the bulk GaAs 43

4.2.2 The thermal conductivity of thin film SiO_2 45

4.2.3 The discrepancy between the measured 2-omega data and simulated 2-omega analysis data on the controlled sample 50

4.3 Superlattice samples 53

4.3.1 GaAs/AlAs 2/2 nm superlattice and 2/8 nm superlattice data analysis method 53

4.3.2 The GaAs/AlAs 2/2 nm superlattice results and discussions 55

4.3.3 The GaAs/AlAs 2/8 nm results 57

4.3.4 Comparison of thermal conductivities of GaAs/AlAs from our research with previous results 59

4.4 Conclusions and summary of this chapter 60

Chapter 5 Conclusion and Future Work 62

5.1 Purpose of this chapter 62

5.2 Summary of the research/thesis and conclusions 62

5.3 Problems or challenges 64

5.4 Future work 65

5.5 Summary 68

References 69

Appendix A 74

Appendix B 76

LIST OF FIGURES

Figure 1.1 The thermal conductivity of superlattice GaAs/AlAs from different studies 14

Figure 2.1 Schematic diagram of 2-D heat profile 17

Figure 2.2 Schematic diagram of the 3-omega method 22

Figure 2.3 The geometry of the FEM model: Notice that the 3-omega model has only one metal line serving as both heater and thermometer and that the 2-omega model has the heater and thermometer separately. 24

Figure 2.4 The schematic diagram of the 2-omega method idea 26

Figure 2.5 The temperature profile vs. frequency.. 27

Figure 3.1 The schematic diagram of the cross-section of the controlled sample 30

Figure 3.2 The Schematic diagram of the superlattice sample 31

Figure 3.3 The schematic diagram of the GaAs/AlAs 2/8nm superlattice 32

Figure 3.4 The schematic diagram of the GaAs/AlAs 2/2nm superlattice structure ... 32

Figure 3.5 The schematic diagram of the 3-omega method.. 33

Figure 3.6 The schematic diagram of the actual experimental setup of the 3-omega method 34

Figure 3.7 The schematic diagram of the 2-omega method [11] 37

Figure 3.8 Peltier module... 39

Figure 3.9 Schematic diagram of the TCR measurement setup.................................. 39

Figure 4.1 The thermal conductivity of GaAs 44

Figure 4.2 Matching example: FEM 3-omega matches the experimental results significantly when choosing proper SiO_2 thermal conductivity; AB54 is the device name that we used to differentiate the devices in our study. 46

Figure 4.3 Thermal conductivity of thin film SiO_2 vs. dimensions 48

Figure 4.4 The deviation from Fourier Law (FEM 2-omega model). The star indicates the average difference between experiment and FEM corresponding to different CC-spacing. All the experimental values are bigger than the FEM values. The error bar shows the maximum and minimum difference. The solid line aids in reading the figure. 52

Figure 4.5 (a) Left: 3-omega data matching and (b) Right: 2-omega data matching; the thermal conductivity is a value in the range between 0.373 and 0.643 [W/m*K]. This figure is an example, and all of the matchings in the study are similar to this figure. 54

Figure 4.6 The thermal conductivity of the GaAs/AlAs 2/2 nm 2 µm thick superlattice. This is plotted depending on the thermal conductivity of the SiO between its minimum and maximum limits..55

Figure 4.7 Anisotropy of the GaAs/AlAs 2/2 nm 2 µm thick superlattice 56

Figure 4.8 Thermal conductivity of GaAs/AlAs 2/8 nm 2 µm thick superlattice........57

Figure 4.9 Anisotropy of GaAs/AlAs 2/8 nm 2 µm thick superlattice 58

Figure 4.10 Comparisons of thermal conductivities GaAs/AlAs superlattice from different periods, thicknesses, and methods 60

Chapter 1 Introduction

1.1The purpose of this chapter

The goal of this chapter is to show the meaning, application, and challenges of superlattice thermal conductivity research as well as the reason why we conducted our experimental research. A detailed literature review on the recent techniques and results of superlattice thermal conductivity is then provided. In the final section, the entire thesis is overviewed.

1.2 Background – meaning, challenge of superlattice thermal conductivity study, and our research

The investigation of the thermal conductivity of superlattices has essential meaning in improving the performance of thermoelectrics and optoelectronics. The research on thermal properties of superlattices has increased since the late 1980s. However, accurate experimental data on the anisotropic thermal conductivity of superlattices are limited, and effective measurement techniques are still under investigation. Our research uses a recently developed technique to measure the anisotropic thermal conductivity of superlattice GaAs/AlAs thin films, named the 2-omega technique, which originates from a widely used isotropic thermal conductivity measurement method, the 3-omega technique. Through combining the 3-omega technique and 2-omega technique, both in-plane and cross-plane thermal conductivities of GaAs/AlAs superlattice thin films are conveniently obtained. In this section, we will address the practical applications and challenges of the research on superlattice thermal properties as well as a brief summary of our research.

1.2.1 Applications of the superlattice

A. Thermoelectrics

In recent years, pollution has gradually affected our global environment, daily lives, and physical health; therefore, society as a whole, especially scientists, has been pursuing environmentally friendly and energy efficient technology. Many research groups have been conducting significant green technology research, named thermoelectrics [1, 3–5], which can directly interconvert electrical energy and thermal energy. Globally, approximately 90% of electrical energy is converted from heat energy [4], but much of the heat is wasted during the energy conversion process. For example, a simple steam cycle for power generation has approximate Carnot efficiency of 50% [2]. The theoretical Rankine efficiency in difference cycles of power generations is between 40%–56% (the real plant values will be lower) [2]. In addition, waste heat is also generated in many modern devices, such as cars [5], computers, and cell phones. Thus, if we could harness this heat and covert it directly to voltage difference, the efficiency of energy use could be improved.

However, thermoelectrics is not as popular as solar cells due to its low efficiency, which is measured by the figure of merit, *ZT*, defined by the following:

$$ZT = \frac{\sigma S^2}{k} T \tag{1.1}$$

where σS^2 is the power factor, and k is the thermal conductivity. For bulk materials, the best *ZT* is approximately 1, which is too low to compete with traditional power generation technology. Much research is dedicated to optimizing the figure of merit *ZT*.

According to the equation, the increase of the power factors or the reduction of the thermal conductivity could increase the figure of merit.

Starting in the early 1990s, the research group of Dresselhaus [6] reported that low dimensional materials could significantly increase the efficiency of thermoelectrics by reducing the thermal conductivity. Later, a great amount of research was conducted on low dimensional materials, such as nanowires, superlattices, and the quantum dot [1–3]. Additionally, research reports that significant reduction in the superlattice thermal conductivity leads to it being one of the best materials for thermoelectrics [7]. In our research, superlattice thermal conductivity also shows a dramatic reduction compared to its corresponding bulk materials.

B. Optoelectronics and other applications

Obviously, the most direct benefit from researching the thermal conductivity of superlattice is the improvement in the efficiency of thermoelectrics, making it practical in more applications. However, these investigations also have broader significance. In the late 1990s, some groups found that research on the thermal property of the materials also plays an essential role in temperature control in many electronics, especially optoelectronics (such as lasers), whose performance is very sensitive to temperature [8]. Recent research shows that the experimental parameters are lacking in the superlattice thermal properties in the design of the nanolaser, which are valuable in the accurate thermal analysis of the nanolaser [9].

1.2.2 The challenge of superlattice thermal conductivity research

A superlattice is a two-dimensional structure that is built by the periodical layers of two or more different materials whose period thickness is around several nanometers.

The thermal conductivity of the superlattice shows an anisotropic property due to its particular structure. The biggest challenges in conducting research on the thermal conductivity of superlattices are experimentally obtaining the precise anisotropic thermal conductivity of the material and developing a practical and efficient experimental method. Very limited anisotropic thermal conductivities in the semiconductor superlattice have been reported although some experimental data on either in-plane direction or cross-plane direction have been published from different research groups. The details of the techniques and results on the superlattice thermal conductivity research are reviewed in section 1.3 of this chapter.

1.2.3 Our research

Inspired by the superlattice's contribution to thermoelectrics and the optoelectronics [1–3, 8–9, 14–15, 23] and the need for more experimental data on superlattice anisotropic thermal conductivity, our group started conducting research related to the thermal property of superlattices. Researchers in our group developed a 2-omega technique and corresponding Finite Element Method (FEM) model, which succeeds in extracting the anisotropic thermal conductivity of bulk materials [10–11]. We applied this newly developed technique to our current superlattice study after predictions by numerical simulations, and we combined it with a traditional 3-omega technique [12] to extract the anisotropic thermal conductivity. In this research and thesis, we measured two samples with 2 μm thick GaAs/AlAs superlattice thin film, whose superlattice periods are 4 nm and 10 nm, respectively. The thermal conductivities in both in-plane and cross-plane directions and the anisotropy are explored and obtained, and challenges we met in this study, such as the sensitivity to the dioxide

thermal conductivity in the 3-omega technique, are explored to further improve our technique.

1.3 Techniques for measuring the anisotropic thermal conductivity of the superlattice and their results in recent research

In this section, we summarize the experimental methods for measuring the semiconductor superlattice thermal conductivities and the corresponding research results.

The primary experimental techniques to explore the thermal conductivity of the superlattice are the 3-omega method, the two-varying-wire 3-omega method, transient thermal grating (TTG), time-domain thermoreflectance (TDTR), or a combination of these techniques. Very limited experimental research results have been reported on the anisotropic superlattice thermal conductivities (both in-plane and cross-plane properties), and some experimental results on the one-direction or average thermal conductivity of the superlattice, such as Si/Ge superlattice and GaAs/AlAs superlattice, have been reported since the late 1990s. The semiconductor superlattice shows complicated thermal properties. In general, the thermal conductivity of the superlattice is much smaller than that of the equivalent bulk materials and has close relations with the period thickness [13–18, 20, 23].

1.3.1 3-omega method and two-varying-wire 3-omega method

A. 3-omega method

The 3-omega method has been intensively used to measure the thermal conductivity of thin film and bulk materials due to its simplicity [12–16]; its use in exploring the Si/Ge superlattice thermal conductivity started when the superlattice

became attractive in the thermoelectrics and optoelectronics [13-16]. This technique is used to measure the average thermal conductivity or the cross-section thermal conductivity of the Si/Ge superlattice [13, 14]. In the 3-omega technique, a metal line is deposited on the surface of the investigated sample, serving as both heater and thermometer. A sinusoidal current passes through the metal line, causing a sinusoidal heat penetration into the sample. Then it generates a temperature oscillation on the surface of the sample (metal line) and a corresponding voltage change of the metal line. The thermal conductivity of the investigated sample is then obtained by building the heat diffusion equation and the measurement of the third harmonic voltage of the metal line. The theory of the 3-omega technique is described in further detail in Chapter 2.

In Lee's research [13], the thermal conductivity of Si/Ge superlattice is measured with periods (L) from 3 nm to 30 nm, and total film thickness from 0.9 µm to 1.8 µm by the 3-omega method. In addition, the thermal conductivity of the order 5 W/m*K at 300 K is reported. These data show very low thermal conductivity in the superlattice, which is smaller than the $Si_{0.85}Ge_{0.15}$ alloy. The research also shows that the thermal conductivity has relations with the periodic thickness, L. The thermal conductivity decreases with decreasing L for $3\ nm < L < 7\ nm$; however, it shows the opposite trend when $L > 13\ nm$. Lee suggests that this unexpected result is probably explained by the formation of the dislocations. However, the thermal conductivity of the superlattice might have a minimum value according to some recent simulations [28, 29]. In summary, this research reports a great reduction of superlattice Si/Ge thermal conductivity compared with that of the related bulk material and smaller than that of the equivalent alloy. However, it does not analyze any thermal properties based on the in-plane or cross-plane direction.

Barca-Tasciuc's group [14] reports on the cross-section thermal conductivity of a symmetrically strained Si/Ge superlattice in the temperature range from 80 K to room temperature by using the 3-omega method. The 30 µm width heater/thermometer is used to measure an approximately 0.5 µm thick superlattice, and the report does not mention if the results are affected by the electricity insulation layer (SiNx), which is an important concern in our current study. Their data show the experimental uncertainty of the thermal conductivity and a reduction of thermal conductivity at larger periods. The specific thermal conductivity of the period 4.4 nm at room temperature is around 4 W/m*K. The relations between thermal conductivity and the sample period are complicated and not fully understood according to Barca-Tasciuc's explanation. Therefore, we can see that 3-omega could approximately measure the cross-plane thermal conductivity of a Si/Ge superlattice, which also shows some complicated relations with the sample periods and the reduction of the thermal conductivity compared to that of the bulk materials.

B. Two-varying-wire 3-omega method

The first experimental results on the temperature-dependent in-plane and cross-plane thermal conductivity of a symmetrically strained Si/Ge superlattice are achieved by the two-varying-wire 3-omega method [15, 16].

A pair of 30µm and 2µm wide heater/thermometer is used to explore both the in-plane thermal conductivity and cross-plane thermal conductivity of the Si/Ge superlattice, and the total thickness of the superlattice is 1.2 µm with a 2/2 nm period (300-period Si [2 nm]/Ge [2 nm]layer) [15, 16]. A 100 nm SiN_x layer is deposited to insulate the electricity leakage. The 30 µm heater is used to measure the cross-plane

thermal conductivity (k_z), because the heat can be assumed to spread in one-direction (down to the substrate). The 2μm wide heater can be used to determine the in-plane thermal conductivity (k_x), because the heat spreads inside the film. The two-dimensional heat conduction model is used to find the in-plane and the cross-plane thermal conductivity after obtaining the related measured data. The measured result is in-plane thermal conductivity k_x 6.3W/m*K and cross-plane thermal conductivity k_z 1.6W/m*K at room temperature, which clearly leads to a big anisotropy (k_x/k_z). The study also shows that the in-plane thermal conductivity is similar to that of the equivalent alloy ($Si_{0.5}Ge_{0.5}$ bulk) level and the cross-plane thermal conductivity is lower than that of the equivalent alloy level. The disadvantage of this method is its uncertainties. For the strained superlattice sample, the uncertainties in the in-plane and cross-plane directions are 20% and 10%, respectively. Therefore, more investigations on this method are needed, but these reported experimental data are still valuable in the study of the superlattice thermal transport.

1.3.2 AC calorimetric method

The AC calorimetric method is the earliest method used to investigate the thermal properties in semiconductor superlattices [17]. This method provides a way to measure the thermal diffusivity parallel to a free-standing thin film, which means that only the in-plane thermal conductivity is measured [17–18]. In this method, a sample is heated by the light partially, and the other part of the sample is covered by a mask, leading to an AC temperature change along the thin film. The AC temperature change of the sample is governed by the heat conduction equation; the heat diffusivity can be achieved by its relation with the amplitude of the AC temperature signal. Finally, the

thermal conductivity can be achieved from the measured thermal diffusivity by the equation $k=\alpha\rho C$, where α is the thermal diffusivity, ρ is the density, and C is the heat capacity. The details of the experiment system and principles are described in Hatta's paper [18, 19].

Yao reports on the first experimental research on the thermal properties of a semiconductor superlattice by the AC calorimetric method [17]. The samples are GaAs/Al superlattices, and the light source used in the measurement is a halogen lamp. The period thickness of the samples varies from 10 nm to 100 nm, and the total sample thickness is 10 µm.

Yu and Chen report on the temperature dependence of the thermal conductivity of GaAs/AlAs with period 70/70 nm by an AC calorimetric technique [18]. The total superlattice thickness is approximately 1µm. The interface scattering is suggested as the primary contribution to the observed reduction of the thermal conductivity in their research.

Their results could not get a clear dependence on the period thickness, but they also show the reduction of in-plane thermal conductivity compared to that of their equivalent bulk material. Their results by the AC calorimetric technique are summarized in Table 1.1 and are also included in Figure 1.1.

Table1 the superlattice thermal conductivity from AC calorimetric technique

The free-standing GaAs/AlAs thin film by the AC calorimetric method at room temperature						
Period (nm)	**10 [17]**	**20 [17]**	**40 [17]**	**60 [17]**	**100 17]**	**140 [18]**
In-plane Thermal conductivity (W/m*K)	**13**	**18**	**32**	**27**	**25**	**41**

1.3.3 Optical pump-and-probe method (or time-domain thermoreflectance [TDTR]), transient thermal grating method (TTG), and their combination

A. Optical pump-and-probe method or time-domain thermoreflectance (TDTR)

According to Capinskin et al., the AC calorimetric technique uses a free-standing plate, which increases the difficulty of sample preparation, and it measures only the in-plane thermal conductivity [20]. Therefore, in Capinskin's experiments, they use an optical pump-and-probe technique to measure the cross-plane thermal conductivity of GaAs/AlAs superlattice. In this method, a metallic film is deposited on the top of the sample. A pump light pulse is focused on the surface of the sample, causing the temperature to rise. The temperature changes and subsequently generates a change in the optical reflectivity. A time-delayed probe pulse is focused on the surface and measures the transient reflectivity of the metal surface. The measured reflectivity is fitted to a numerical model by adjusting the thermal conductivity of the superlattice.

Because the spot size is bigger than the thermal penetration depth, the heat primarily propagates perpendicular to the superlattice film. Therefore, the optical pump-and-probe method [20–23] is always used to evaluate the cross-section thermal conductivity of the superlattice, and it is also called time-domain thermoreflectance (TDTR) [23]. More details about this method can be found in Capinskin and Schmidt's research [21, 22].

Capinskin et al. report that the cross-section thermal conductivities of GaAs/AlAs vary from approximately 4 W/m*K to 14 W/m*K with the period from 0.3 nm to 13 nm and the total thickness of the superlattice from 212 nm to 849 nm. Although they report that the cross-section thermal conductivity decreases as the superlattice period reduces, we could not obtain a strict conclusion about this due to a lack of data and also due to some data in their research not showing this trend, especially at the very small period thickness. The details of the results can be found in Figure 1.1.

B. Transient thermal grating (TTG)

In the TTG [23–27] technique, the optical interference of the two excitation pulses on the sample surface produces a sinusoidal variation in intensity. The absorption of the light induces the heating in the geometry of the optical interference pattern, and the transient thermal grating (the temperature profile) is formed. The temperature profile can be determined by the diffraction of a probe laser beam with a reference beam in a heterodyne detection [24, 25]. Especially, the phase-controlled heterodyne detection is introduced in the measurements of the thermal properties of the opaque material [27] and superlattice [23]. Through analyzing the temperature profile, the thermal properties (such as thermal diffusivities) can be generated. The details of the methodology and

principles are described in the paper by Johnson et al. [27]. Regarding the aspect of analyzing the thermal grating decay, the temperature grating decays are mainly due to in-plane thermal diffusion at short grating periods. Therefore, this technique is used to characterize the in-plane thermal conductivity [23, 27]. In this improved method (the one with the phase control heterodyne detection), no coating is needed on the surface of the superlattice, which eliminates the effect from the thermal boundary resistance at the metal-semiconductor interface. However, this requires the consideration of the presence of photoexcited carriers [23]. The TTG technique on the superlattice thermal conductivity is new, and to our knowledge, only one research group has used this method to measure the in-plane thermal conductivity of the superlattice [23].

C. The combination of the TDTR and TTG techniques

Luckyanova et al. report on the anisotropic thermal conductivity of GaAs/AlAs superlattice; to our knowledge, this is the latest experimental report on the study of both in-plane thermal conductivity and cross-plane thermal conductivity in the semiconductor superlattice [23]. In the paper by Luckyanova et al., the TTG and TDTR techniques are combined to measure the anisotropic thermal conductivity of GaAs/AlAs superlattice. According to their report, the TTG technique is sensitive to the in-plane thermal property, while TDTR is only sensitive to the cross-plane thermal conductivity. A summary of these two methods has been described in sections A and B.

Two samples with a total superlattice thickness 3.5 μm are measured. One is with a 4 nm (2 nm for each layer) period thickness, and the other is with 16 nm (8 nm for each layer). The in-plane thermal conductivities for the two samples are around 8.05

W/m*K (2/2 nm sample) and 11.4 W/m*K, respectively; the cross-plane thermal conductivities for the two samples are 6.5 W/m*K (2/2 nm sample) and 8.7 W/m*K, respectively. The researchers [23] suggest that thermal conductivities increase as the period increases, according to the data fit from all the measured GaAs/AlAs data so far. However, some other researchers have suggested that the thermal conductivity has a minimum at some period [28, 29], and the experimental data described above have different predictions, so the trend of the thermal conductivities related to the period thickness requires more reliable experimental data.

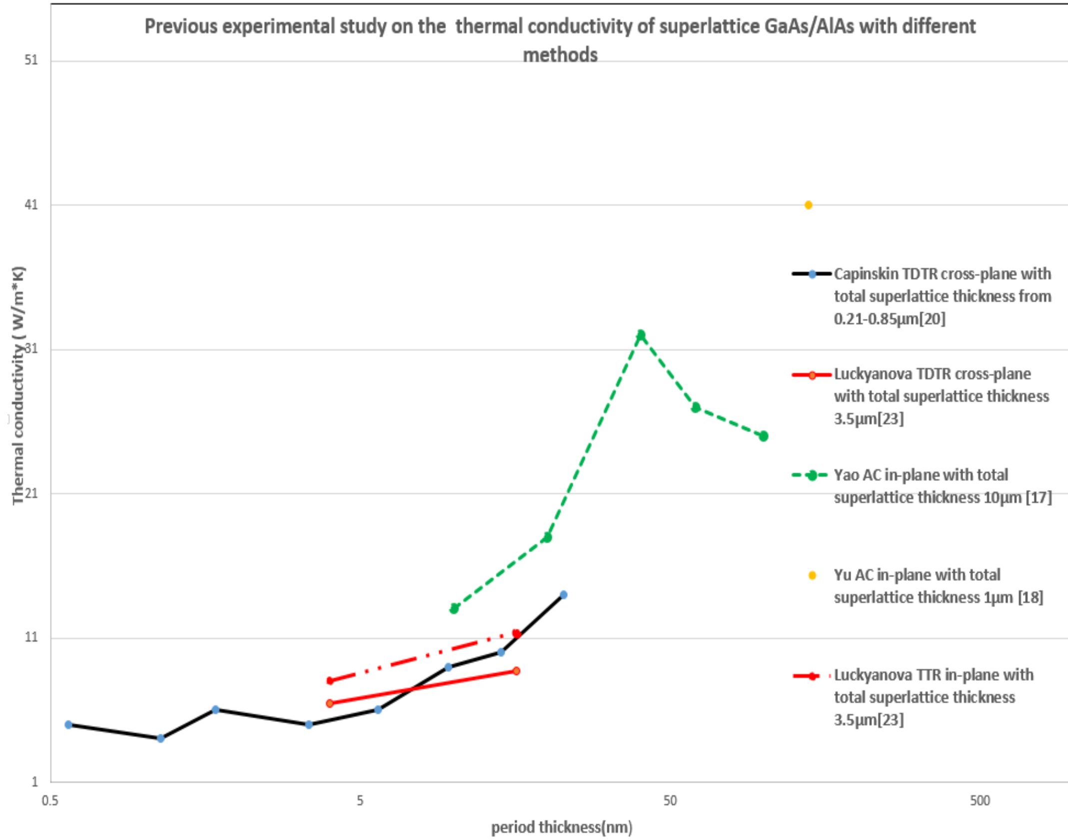

Figure 1.1 The thermal conductivity of superlattice GaAs/AlAs from different studies

1.3.4 Summary of the literature review

There is a limited number of reports on the anisotropic thermal conductivity of a semiconductor superlattice, and no methods have proven to be the best candidate to measure the superlattice anisotropic thermal conductivity thus far. Our research focuses on the combination of the 3-omega technique and 2-omega technique to study the anisotropic thermal conductivity of superlattice experimentally due to the simplicity of the experimental setup and the popularity in the measurement of the thermal conductivity of the bulk materials and thin film. We expect to contribute more

experimental data to the superlattice thermal properties research and study the strength and weakness of this method for further research reference. The next section provides an overview of our complete thesis.

1.4 Overview of this thesis

This thesis explores the anisotropic thermal conductivity of superlattice GaAs/AlAs by a combination of 3-omega and 2-omega techniques. Chapter 1 discusses the significance of investigating the thermal conductivity of superlattice and justifications for our research. Then, the chapter gives the literature review and the primary experimental techniques of measuring the thermal conductivity of the semiconductor superlattice and their results. Chapter 2 details the theory of the 3-omega method and the process of how we generated the idea of the 2-omega method. Chapter 3 describes all the methodologies about the measurement of the essential parameters and experimental setups required in this research. Chapter 4 shows the methods of analyzing the collected experimental data, which include analytical formulas and numerical models built by MATLAB®, and the results of the data analysis. Chapter 4 also briefly discusses the results, and it compares the results with data from other researchers. The last chapter, Chapter 5, presents the conclusion of our study on thermal conductivities and anisotropies of superlattice GaAs/AlAs samples and the measurement technique. It also describes possible improvements on this technique for future research.

Chapter 2 Theory of the 3-omega Technique and the Idea of the 2-omega Technique

2.1 The goal of this chapter

This chapter explains the theory of the 3-omega method for substrate thermal conductivity, the theory and the simulation model for the isotropic thin film, and the simulation predictions on the 2-omega method in detail. The derivation of the 3-omega method formula and the FEM simulation of the 2-omega method will be the theoretical foundation for measuring the thermal conductivity of substrate GaAs, thin film SiO_2, and the superlattice thin film layer in this research.

2.2 The 3-omega method

2.2.1 3-omega method for substrate thermal conductivity

The 3-omega method [12] is a common method to measure the thermal conductivity of substrate and isotropic thin film [4, 14–16, 30–32]. We chose this method to measure our sample substrate GaAs. Below, the detailed derivation is given, which refers primarily to Woo Chul Kim's dissertation [4].

A. The schematic diagram and the governing equation

A thin metal line is deposited on top of the material, the thermal conductivity of which is needed to measure. See figure 2.1 below for a schematic diagram. A sinusoidal power is driven into the wire; then, heat is generated and penetrated into the substrate. The proper frequency should be chosen so that the penetration depth is not beyond the thickness of the substrate under the measurement. The width of the line is also much

smaller than the length of it. This makes it so that the cylindrical heat diffusion equation in semi-infinite solid can be used. Equation 2.1 below shows the governed equation to describe this model.

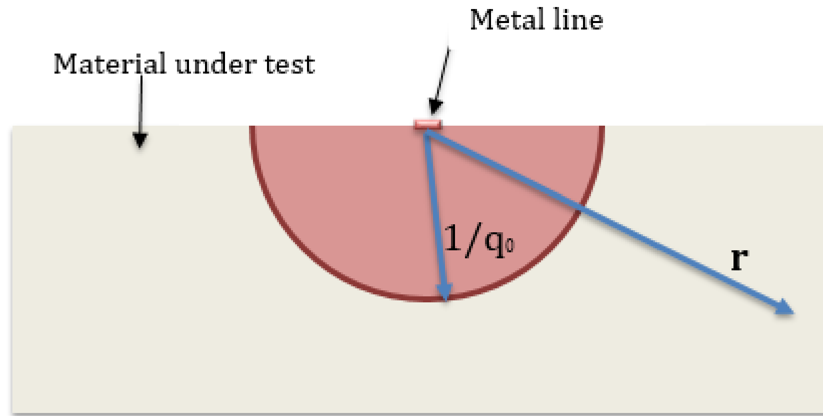

Figure 2.1 Schematic diagram of 2-D heat profile

$$\frac{\partial T(r,t)}{\partial t} = \frac{\alpha_{th}}{r}\frac{\partial}{\partial r}\left(r\frac{\partial T(r,t)}{\partial r}\right) \quad (2.1)$$

where T is the temperature at position r and time t of the substrate, α_{th} is the thermal diffusivity. Because the power driven into the wire is periodic, the temperature is assumed to be in a steady periodic form.

$$T(r,t) = T0 + \Delta T(r) * \exp(i2\omega t) \quad (2.2)$$

In the above equation, ω is the circular frequency of the current driven into the metal line. After inserting the periodic temperature profile into equation 2.1, the equation becomes the form below.

$$\frac{1}{2\omega i/\alpha_{th}}\frac{\partial^2(\Delta T(r))}{\partial r^2} + \frac{1}{2\omega i/\alpha_{th}}\frac{1}{r}\frac{\partial \Delta T(r)}{\partial r} - \Delta T(r) = 0 \quad (2.3)$$

This equation can be written in the simplified form shown in equation 2.4below.

$$\frac{d^2}{dr'^2}\Delta T(r') + \frac{1}{r'}\frac{d\Delta T(r')}{d(r')} - \Delta T(r') = 0 \qquad (2.4)$$

In the equation, *r'* is defined as 2.5 and the thermal penetration is defined as 2.6 below.

$$r' = (\frac{i2\omega}{\alpha_{th}})^{1/2} * r \qquad (2.5)$$

$$\frac{1}{q0} = (\frac{\alpha_{th}}{i2\omega})^{1/2} \qquad (2.6)$$

B. The modified Bessel function and its solution

Equation 2.4 has a similar form to that of the modified Bessel function [33]; the modified Bessel function of order *n* is the following:

$$\frac{d^2y}{dx^2} + \frac{1}{x}\frac{dy}{dx} - \left(1 + \frac{n^2}{x}\right)y = 0 \qquad (2.7)$$

When *n* is zero, 2.4 and 2.7 have the same form. The solution of the modified Bessel function is described in equation 2.8 below [33].

$$y = C_1 I_n(x) + C_2 K_n(x) \qquad (2.8)$$

In the equation, C_1 and C_2 are constant, and $I_n(x)$ and $K_n(x)$ are a modified Bessel function of the first kind and a modified Bessel function of the second kind, respectively. When x increases to infinity, $I_n(x)$ will go to infinity, and $K_n(x)$ will go to zero. Thus, the solution of equation 2.4 can be found through the modified Bessel function of order 0. The temperature profile is the following:

$$\Delta T(r') = C1 I_0(r') + C2 K_0(r') \qquad (2.9)$$

C_1 and C_2 will be solved later through the boundary condition, and $I_0(r')$, $K_0(r')$ are a modified Bessel function of the zeroth order of the first and second kind.

C. The boundary condition and the relations between temperature oscillation and thermal conductivity

The boundary conditions are $\Delta T=0$ as r goes to infinity and

$$P = \lim_{r\to 0}[-k(\pi r l)\frac{d\Delta T}{dr}].$$

According to the first boundary condition, ΔT should be zero as r or r' goes to infinity. When r' goes to infinity, $I_0(r')$ also goes to infinity. Thus, C_1 must be zero. Equation 2.9 is simplified to the following:

$$\Delta T(r') = C2K_0(r') \quad (2.10)$$

According to the second boundary condition and the characteristics of the modified Bessel function of the second kind [33], the constant C_2 is solved, $P=k\pi lC_2$. Then, the temperature profile can be represented as follows:

$$\Delta T = \frac{P}{k\pi l}K_0(q_0 r) \quad (2.11)$$

When the arguments $0 < |x| << (\alpha+1)^{1/2}$ are satisfied, the modified Bessel function of the second kind becomes the following:

$$K_\alpha \sim -\ln\left(\frac{x}{2}\right) - \gamma \; if \; \alpha = 0 \; . \quad (2.12)$$

In the equation, γ=0.5722 (Euler's constant). If we consider only the temperature profile of the surface of the solid, *r* will be close to zero and will be much smaller than the penetration depth $1/q_0$. At the surface, $|q_0 r| << 1$, the temperature profile becomes

$$\Delta T(0) = \frac{P}{k\pi l}[-\ln\left(\frac{q_0 r}{2}\right) - \gamma] \quad (2.13)$$

After plugging the penetration depth into equation 2.6, the surface temperature profile is shown as follows:

$$\Delta T(0) = \frac{P}{k\pi l}[-\frac{1}{2}\ln\left(\frac{\alpha_{th}}{r^2}\right) + ln2 - \frac{1}{2}\ln(2\omega) - \gamma - 1/4i] \quad (2.14)$$

According to Cahill's paper, the in-phase item generates a more reliable result; thus, our work also uses the in-phase temperature profile on the surface of the solid.

If two frequencies are chosen and the in-phase temperature profile equation is used, the differential temperature of the surface can be written as follows:

$$\Delta T(0)_{\omega=\omega 1} - \Delta T(0)_{\omega=\omega 2} = \frac{P}{k\pi l}[\ln(\frac{\omega 1}{\omega 2})] \quad (2.15)$$

Thus, the thermal conductivity of the substrate can be expressed by the temperature oscillation difference at the surface of the substrate, as below.

$$k = \frac{P}{2\pi l} * \frac{\ln(\frac{\omega 2}{\omega 1})}{\Delta T(0)_{\omega=\omega 1} - \Delta T(0)_{\omega=\omega 2}} \quad (2.16)$$

D. The final results of the 3-omega method

The schematic diagram is shown in figure 2.2 on the next page. The sinusoidal current with the circular frequency ω is driven into the metal line through the outer pads, causing the Joule heat to fluctuate in frequency 2ω, creating temperature oscillations everywhere, including the metallic heater. The temperature change will lead

to the change of the resistance of the metal line, which is described by the equation below.

$$R = Ro + Ro * TCR * \Delta T(0) * \cos(2\omega t) \quad (2.17)$$

In the equation, R_O is the resistance at the room temperature. *TCR* is the temperature coefficient of the resistance and is defined as $TCR=1/R_O*(dT/dR)$. $\Delta T(0)$ is the temperature oscillation of the metal line or the surface temperature oscillation of the material under the metal line. Therefore, the voltage of the metal line should be the following:

$$V = I * R = Io * coswt * Ro * (1 + TCR\Delta T(0)\cos(2wt))$$

$$= \left[IoRo + \frac{1}{2} * IoRoTCR\Delta T(0)\right]\cos(wt) + \left[\frac{1}{2} IoRoTCR\Delta T(0)\right]\cos(3wt)$$

$$\cong [IoRo]cos(wt) + \left[\frac{1}{2} * IoRo * TCR * \Delta T(0)\right]\cos(3wt)$$

$$\equiv V_{1\omega} * \cos(\omega t) + V_{3\omega} * \cos(3wt) \quad (2.18)$$

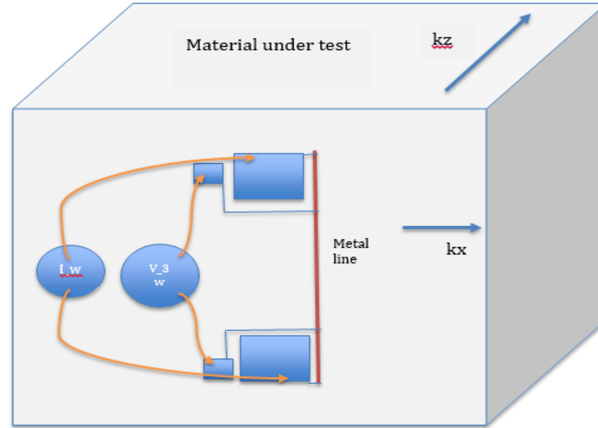

Figure 2.2 Schematic diagram of the 3-omega method

From equation 2.18, we can see that the surface temperature oscillation can be expressed by the amplitude of the third harmonic of the voltage of the metal line, which is listed below.

$$\Delta T(0) = \frac{2V_{3\omega}}{Vo*TCR} \tag{2.19}$$

After substituting (2.19) into equation 2.16, the final expression of the 3-omega method to obtain the thermal conductivity is derived.

$$k = \frac{P}{2\pi l} * \frac{\ln(\frac{\omega 2}{\omega 1})*TCR*Vo}{2*(V_{3\omega,\omega=\omega 1} - V_{3\omega,\omega=\omega 2})} \tag{2.20}$$

This equation is what we will use to calculate the substrate GaAs' thermal conductivity. In our research, the dimension of the metal line is 0.5–2μm wide, 0.5μm thick, and 300μm long; the thickness of the substrate of GaAs is larger than 500 μm. The penetration depth *(1/q)* can be calculated by equation 2.6. The thermal diffusivity is 0.31 cm^2s^{-1}, from the literature [34]. The magnitude of this complex quantity 1/q is approximately 350 μm with 20 Hz, which is smaller than the substrate thickness. The

frequency is set between 20–2000 Hz in the experiment and 90–2000 Hz in the actual calculation, which will ensure that the penetration depth is smaller than the substrate thickness. According to the conditions listed above, the line source is valid in our research, and all the previous derivations and approximations in this chapter can be used.

2.2.2 The 3-omega method to extract the isotropic thin film thermal conductivity and the FEM simulation model

The method we used to obtain the thermal conductivity of the thin film SiO_2, the first layer on the top of the substrate, is still the 3-omega method. In fact, the same experimental data as those for the substrate are used to conduct the data analysis. Instead of using the analytical calculation to get the thin film thermal conductivity extraction, the Finite Element Method (FEM) MATLAB® program from reference 10 is used to obtain the thin film thermal conductivity. The program code can be requested from the authors of reference 10 if desired.

This FEM approach could calculate both in-phase and quadrature temperature profile (TP) directly under a range of frequencies in one simulation by solving the heat equation in the frequency domain. Compared to the time-domain FEM model, this approach does not require other post-processings and is more convenient when a large number of frequencies are demanded. More importantly, it can handle several layers of the thin film. The basic structure is shown in figure 2.3 below. Moreover, this is a 2-D frequency domain FEM implementation; we assume that heat flux mainly goes in the x and z directions in figure 2.3. Thus, to satisfy the 2-D FEM model, only the longest length, 300μm, is measured in the actual experiment and simulations.

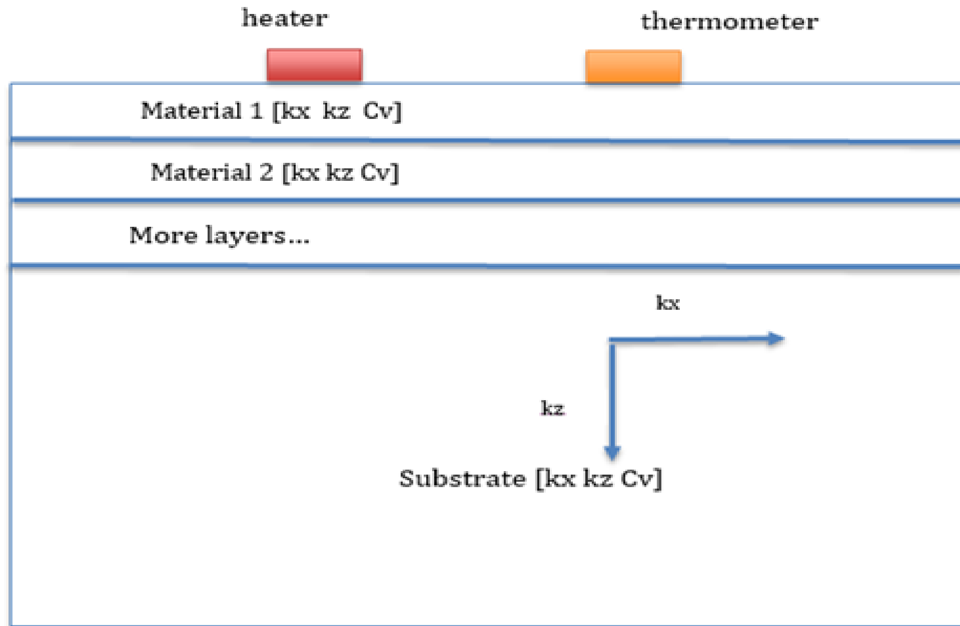

Figure 2.3 The geometry of the FEM model: Notice that the 3-omega model has only one metal line serving as both heater and thermometer and that the 2-omega model has the heater and thermometer separately.

Before running the simulation, the heat capacity C_V and thermal conductivity tensor (equation 2.17) for each material should be specified in the program. The thermal conductivity tensor relative to the coordinate axes shown in Fig. 2.3 is assumed to be a 2x2 matrix with 0 off-diagonal entries:

$$\widehat{K} = \begin{bmatrix} k_x & 0 \\ 0 & k_z \end{bmatrix} \tag{2.17}$$

where k_x is the in-plane thermal conductivity, and k_z is the cross-plane thermal conductivity. Thus, this approach can simulate both the anisotropic and isotropic material. In the case of extracting the SiO_2 thin film thermal conductivity, $k_x = k_z$. Besides the dimensions of the structure, such as the width and thickness of the metal line and all layers, the mesh details and heat source should also be specified.

The specific procedures for extracting the SiO_2 thermal conductivity are listed below. After achieving the thermal conductivity of GaAs by the method described in section 2.2.1, the thermal properties of all materials, dimensions and frequencies, should be inserted into the proper positions. After running the simulation, the temperature profile will be generated. Finally, this simulated temperature profile will be matched with the experimental temperature profile by adjusting the SiO_2 thermal conductivity. When the simulation results match the experimental results, the value of SiO_2 thermal conductivity is achieved.

2.3 The simulation prediction and the idea of the 2-omega method for anisotropic thin film

In the superlattice thermal conductivity measurement, a novel technique, the 2-omega method, is used with the foundation of the 3-omega technique [10, 11]. Instead of using the one metal line serving as both the heater and the thermometer, two metal lines are used. AC power is driven into one metal line, and another metal line serves as a thermometer. The schematic diagram, figure 2.4, is on the following page. This method is expected to distinguish between materials with the same average thermal conductivity but different anisotropy, which could not be accomplished by the 3-omega method through the same device. The average thermal conductivity is defined as $(k_x + k_z)/2$. The anisotropy is defined as k_x / k_z. In addition, according to the geometry shown in figure 2.4, the temperature oscillation of the 2-omega method is expected to be more sensitive to k_x than k_z intuitively. Moreover, the temperature oscillation of the 3-omega should be more sensitive to k_z than k_x if we design the width of the metal line properly. Therefore, combining the 3-omega method and 2-omega method, we should be able to

extract the thermal conductivity k_x and k_z in the anisotropic superlattice. The combination of the 2-omega and 3-omega methods has shown to be valid in the thick film in the previous work on 500 µm rutile TiO_2. However, no experiments have been conducted on the anisotropic thin film with this new technique [11]. Below, we show how we predict the validity of the 2-omega method in the thin film materials by FEM model. The FEM model is the same as that introduced in section 2.2.2. The main difference is that the geometry has two metal lines, serving as heater and thermometer separately.

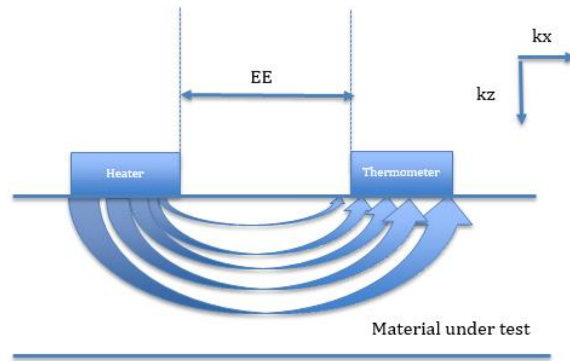

Figure 2.4 The schematic diagram of the 2-omega method idea

The FEM 2-omega simulation model is used to predict the validity of the 2-omega technique. The 2 µm thickness thin film is on the top of the substrate, which is 500 µm in the simulation. The metal lines are 300 µm long and 0.5 µm wide and are separated by 2 µm edge from edge. They are designed to be thin enough to satisfy the line source approximation as used in the 3-omega method. Four materials with different thermal properties are simulated, whose thermal conductivities are { k_x =20 W/m*K, k_z= 10 W/m*K}, { k_x =15 W/m*K, k_z= 15 W/m*K},{ k_x =10 W/m*K, k_z= 10 W/m*K}, and { k_x =20 W/m*K, k_z= 20 W/m*K}. One reason we choose a number between 10 and 20

W/m*K is that some experimental research shows that GaAs/AlAs superlattice thermal conductivity with 2 μm thickness gave results close to this range [23]. Therefore, we assume that our experimental results are close to this result and expect 2-omega FEM simulations to work well in this range. The simulated results are shown in figure 2.5 below.

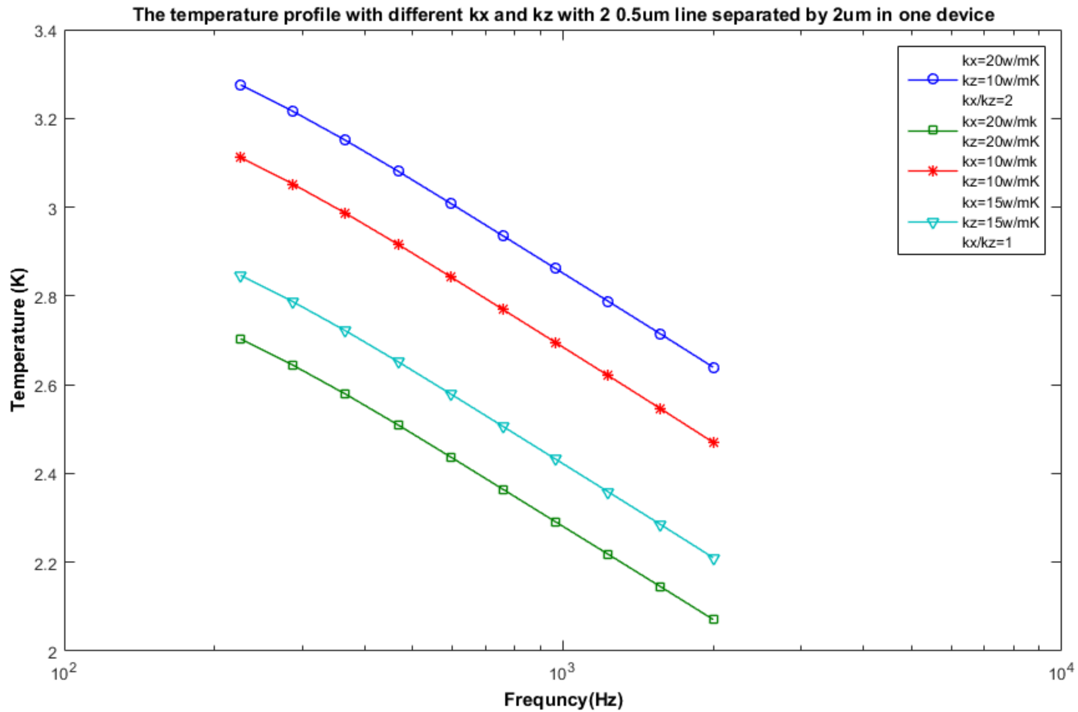

Figure 2.5 The temperature profile vs. frequency

A. Anisotropy sensitivity

From figure 2.5, it can be seen that the thin film 2-omega FEM model temperature profile is very sensitive to the anisotropy. Although the circle curve and the triangular curve have the same average thermal conductivity, 15 W/m*K, these two curves show different temperature profiles obviously in a large range of the frequencies due to their different anisotropy, 2 and 1 separately.

B. In-plane k_x and cross-plane k_z sensitivity

This 2-omega method is expected to be more sensitive to k_x. However, figure 2.5 shows that the temperature profile of this model is more sensitive to k_z in the 2μm case. However, this will not affect the use of the 2-omega method to explore the anisotropy, because simulations show that the 2-omega model is still sensitive to k_x when the thin film is 2 μm in thickness.

From the predictions of the 2-omega FEM model, the idea of combining the 2-omega method and 3-omega method to obtain the thermal conductivity and anisotropy of the superlattice is generated. In the actual data analysis, the simulation results will be adjusted to match the experimental results by changing the k_x and k_z. When both the simulations of 2-omega and 3-omega match the experimental results, both the thermal conductivities and the anisotropy are achieved.

2.4 Summary and conclusion

This chapter describes the theoretical background, simulation models, and predictions to extract the thermal conductivity of substrate GaAs, SiO_2 thin film, and superlattice thin film. It gives the complete theoretical derivations of the 3-omega method, which is the method we used to extract the thermal conductivity of the substrate GaAs and some sort of directionally averaged thermal conductivity of the thin film on it. Then, we introduced the FEM simulation model, which is used to conduct the data analysis of the isotropic thin film and the superlattice film. This FEM model also assists us with the idea of the 2-omega method to extract the anisotropy of the superlattice. Therefore, the theoretical derivations or simulation predictions have been built to explore the superlattice thermal conductivity and anisotropy in this chapter.

Chapter 3 Experimental Methodology

3.1 The purpose of this chapter

This chapter aims to describe the experimental methodologies used in our research, including the sample preparation and the devices' measurements. The basic structures of the samples and methods to fabricate them will be described in section 3.2 and Appendix A. The 3-omega technique and 2-omega technique experimental setups and the measurement methods of related essential parameters will be detailed in section 3.3.

3.2 The sample preparation

Three samples were used in this research. The first was the controlled sample, which includes only substrate GaAs and thin film SiO_2. The substrate GaAs and the SiO_2 film of the controlled sample were designed to process to have the same property and dimensions as those in the superlattice samples. By measuring the thermal conductivities of the GaAs and SiO_2 in the controlled sample, the parameters of the superlattice samples can be obtained indirectly. The other two samples were GaAs/AlAs superlattice with periods 2/2 nm and 2/8 nm, respectively.

3.2.1 The controlled sample

In the controlled sample, a 68 nm thick SiO_2 film was deposited on a clean, double-sided, polished 2-inch diameter unintentionally doped GaAs wafer by plasma-enhanced chemical vapor deposition (PECVD) at 248 ℃. Then, two 20/500 nm thick Ti/Al metal lines were deposited on the top of the SiO_2 film. The edge-to-edge separation (E-E) between the two lines was 500 nm, 1000 nm, and 2000 nm. The width

of the line was between 500 nm and 2000 nm. Our target thickness of the SiO_2 film was 50 nm, which is the same as the dioxide thickness in the superlattice samples. However, it was measured using an Ellipsometer at 68 nm thick on the controlled sample – the variation in the fabrication process was due to undetermined causes. The schematic diagram of the controlled sample is given in figure 3.1.

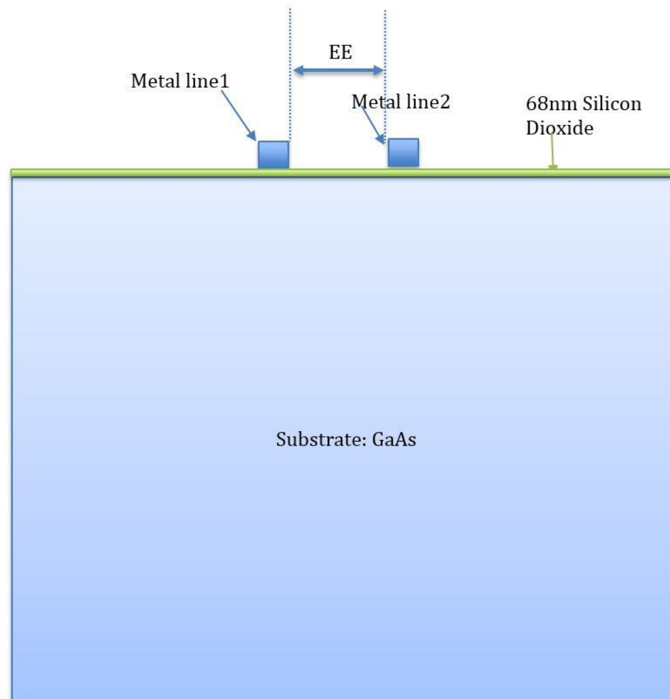

Figure 3.1 The schematic diagram of the cross-section of the controlled sample

3.2.2 Superlattice samples

During the fabrication process of the superlattice, the samples were grown on native (100) GaAs substrates at 600 °C following a 10 min oxide desorption under As overpressure at 610 °C. Growth was initiated with a 200 nm GaAs buffer followed by the superlattice structures. The thickness of the superlattice was 2um. One sample was

2nm GaAs and 2nm AlAs period, repeated 500 times. Another sample was 2nm GaAs, followed by 8nm AlAs, repeated 200 times. After fabricating the superlattice structure, the sample was processed to deposit a 50 nm SiO_2 thin layer by PECVD at 248 ℃ and 20/500 nm Ti/Al metal lines. The details of the fabrication of the superlattice are in Appendix A. The schematic diagram of the structure of the superlattice samples is shown in figure 3.2. Additionally, figure 3.3 and figure 3.4 show the two structures of the superlattice in our research.

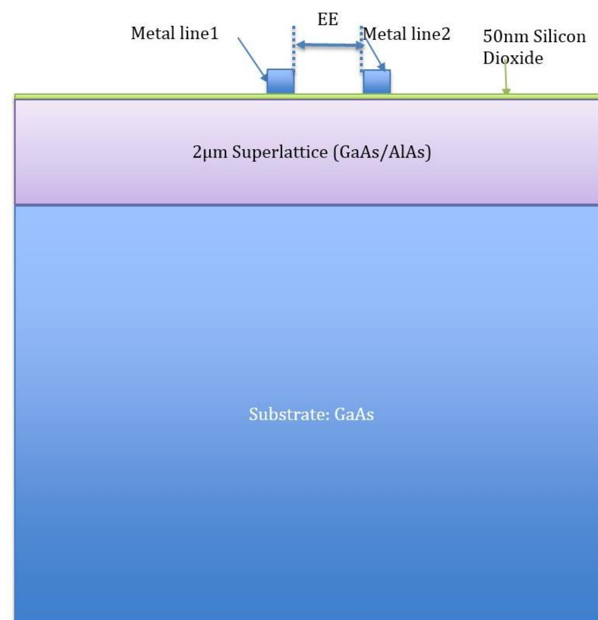

Figure 3.2 The Schematic diagram of the superlattice sample

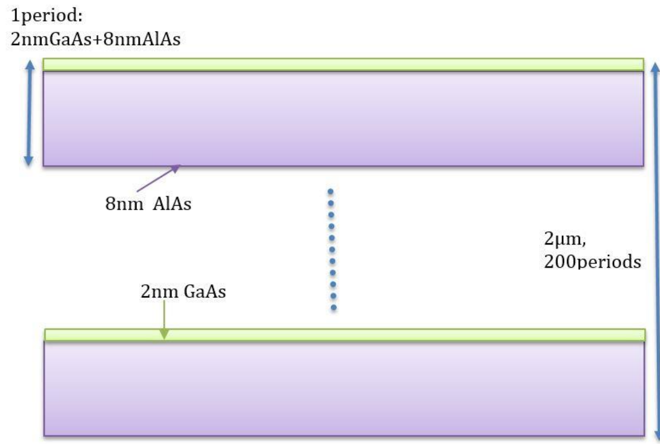

Figure 3.3 The schematic diagram of the GaAs/AlAs 2/8nm superlattice structure

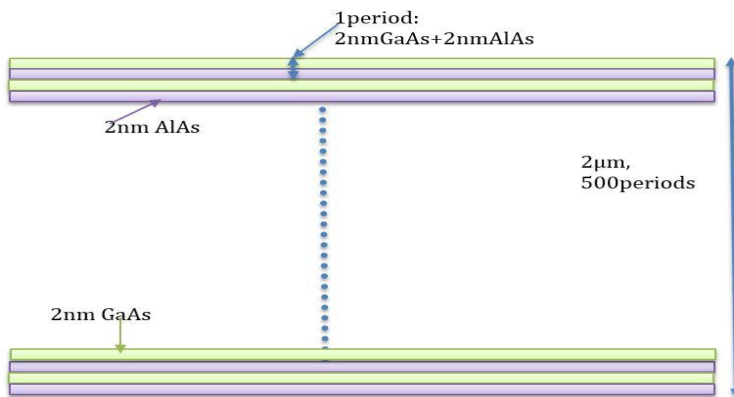

Figure 3.4 The schematic diagram of the GaAs/AlAs 2/2nm superlattice structure

3.3 Experimental setups and procedures

The main experimental setups of this research are 3-omega and 2-omega techniques, both of which were applied to the controlled wafer and the superlattice

wafers. The details of the experimental methodology applied to the controlled sample will be described in sections 3.3.1 and 3.3.2. Moreover, the superlattice experimental setups followed the same design as the controlled sample, which will be summarized in section 3.3.3. Furthermore, TCR (temperature coefficient of the resistance) and the actual device dimension measurements will be shown in section 3.3.4.

3.3.1 The experimental setup of the 3-omega technique on the controlled sample

The purpose of applying the 3-omega technique on the controlled sample is to extract the thermal conductivities of the substrate GaAs and thin film SiO_2. Figure 2.2 in Chapter 2 shows how the metal line serves as both the heater and the thermometer. Electrical connections to the metal line were accomplished by the probes that contacted the outer and inner pads on the metal line. The length of the metal line is 200µm and

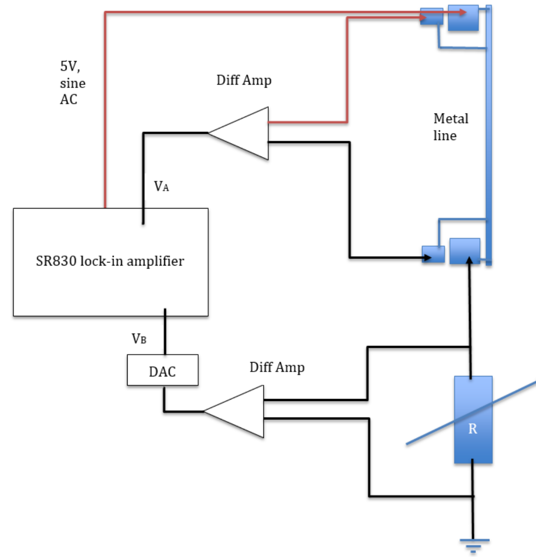

Figure 3.5 The schematic diagram of the 3-omega method

300µm; the width of the line is approximately 1 µm and 2 µm. Our experiment was conducted at room temperature.

Figure 3.5 shows the complete schematic diagram of the 3-omega method. The SR830 lock-in amplifier was used to afford the 5V sinusoidal AC source and measure the first and the third harmonic of the voltage across the metal line. From equation 2.18, both ω and 3ω are present across the metal line, and the ω is around 1000 times bigger than the 3ω component [12]. To measure this small third harmonic voltage, the first harmonic voltage should be removed. Thus, a potentiometer was connected in series with the metal line to eliminate the ω voltage [4, 12]. The resistance of the metal line was measured by the four-wire sensing method. A small current (5 groups within -300 to 300 mA) was forced to the outer pads of the metal line, and the multimeter was connected to the inner pads to sense the voltage. Then, the resistance was obtained by plotting the relations between the voltage and the current; the slope was the metal line resistance. The measurement of TCR was done after all experiments had been finished on the controlled sample; the details will be introduced in

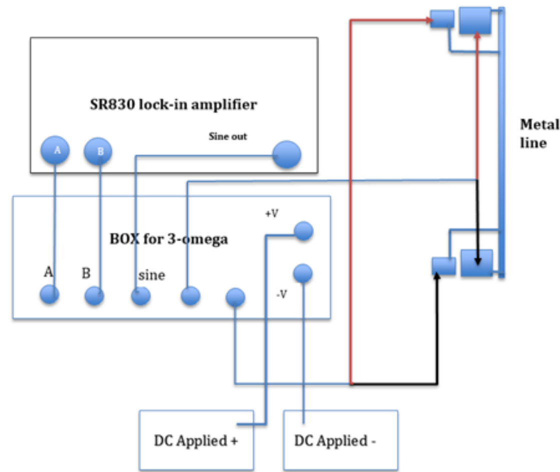

Figure 3.6 The schematic diagram of the actual experimental setup of the 3-omega method

section 3.3.4. The output voltage of the SR830 to heat the metal line was with an amplitude of 5V and frequencies ranging from 20 Hz to 2000 Hz (90-2000 Hz was used in the calculations in data analysis). In all the experiments, it was essential to make sure the contacts between the probes and pads were stable and effective. Figure 3.6 is the actual experimental setup of the 3-omega method, where all the circuits were built in box 1.

3.3.2 The 2-omega technique experimental methodology on the controlled sample

The 2-omega technique was applied to the controlled sample to investigate the deviation of the experimental 2-omega results from the FEM 2-omega model (based on Fourier's Law). This investigation could also be used to correct the 2-omega FEM model of the superlattice to improve the accuracy of the superlattice data analysis. Instead of using the same metal line as the heater and thermometer, a separated metal line with the same dimension of the heater was used to sense the temperature oscillation, as described in Chapter 2; only the in-phase temperature was used, as in the 3-omega method [11]. An AC current was driven into the heater, which caused the temperature oscillation at the 2ω on the surface of the sample; thus, the temperature of the thermometer oscillated at a 2ω frequency. According to equation 2.17, the resistance of the thermometer also oscillated at the 2ω frequency. While a DC current passed through the thermometer, the voltage across the thermometer line was

$$V_{therm} = I_{DC} * [R_{o_thermo} * (1 + TCR * \Delta T(0) * \cos(2\omega t))] = V_{DC} + V_{2\omega} ,$$

(3.1)

where R_{O_thermo} is the resistance of the thermometer at room temperature. The DC component was filtered by a capacitor, and $V_{2\omega}$ was measured by the lock-in amplifier.

The actual experimental setup is described in figure 3.7. The 5V sinusoidal AC source was driven into the outer pads of the heater loop. A 100k resistor was connected between the source and the metal line to reduce the noise pick-up at the connection [11]. A voltage meter was connected to the inner pads of the heater to measure $V_{1\omega}$, which would be used to determine the input heating power. Instead of feeding the DC current directly to the thermometer, a voltage source V_{DC} was driven across a series combination of a 1000 resistor and the thermometer line. The DC current was calculated by (V_{DC}-V_{thermo})/1000, where V_{thermo} was measured by the voltage meter connected to the inner pads of the thermometer. After measuring V_{thermo}, the SR830 lock-in amplifier was connected to the inner pads of the thermometer to measure the $V_{2\omega}$ and the DC voltage across it was eliminated by a capacitor in the lock-in amplifier. The frequency was swept from 20 to 2000 Hz (data from 225-2000 Hz was used in the data analysis), and $V_{2\omega}$ of the thermometer and $V_{1\omega}$ of the heater were obtained during the experiments. Then, the voltage was converted to the in-phase temperature oscillation profile by a proper equation [11]. The detailed data analysis on these measured parameters will be given in Chapter 4.

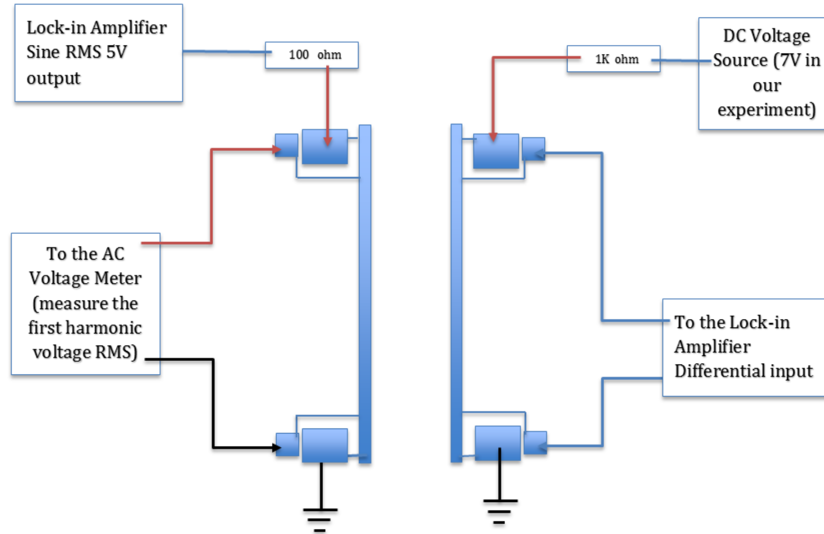

Figure 3.7 The schematic diagram of the 2-omega method [11]

3.3.3 3-omega and 2-omega set-ups for the two superlattice samples

The experimental setups of the 2-omega method and the 3-omega method were the same as those described in sections 3.3.1 and 3.3.2 except for the devices that we chose to measure in the 2-omega experiment. Only devices that are 0.5µm wide, 300µm in length, and separated by a 2µm edge to edge of the metal lines were measured by the 2-omega technique. The reason only 2µm separations were chosen was because they had the lowest deviation of the FEM model simulation results from the experimental results, and the error could be greatly reduced in the data analysis. The details will be given in Chapter 4. The experimental setups of the superlattice samples are shown in figure 3.6 and figure 3.7.

3.3.4 Other parameters: Real dimensions of the devices and TCR of the metal line

A. The dimension of the metal line

To improve the accuracy of the data analysis, we measured the actual width of the used metal lines and edge-to-edge separation of the two metal lines by a scanning electron microscope (SEM).

B. TCR measurement

When all other measurements were finished, the TCR measurement could be conducted. Temperature Coefficient Resistance (TCR) is defined by the equation $TCR=1/R_O*(dT/dR)$. R_O is the metal line resistance at room temperature, and T is the temperature of the metal line. We used the Peltier module to generate five different temperatures. The Peltier module transfers heat from one side to the other when a current is driven through it. The temperature difference of the device is decided by the amplitude and direction of the current running through it and by its thermal coupling to the surroundings. See figure 3.8 for the Peltier module. The thermal paste was spread on the surface of the Peltier module. Then, the wafer was put on the top of the thermal paste so that the temperature change of the Peltier module could cause the temperature change of the wafer. The four-wire sensing method was used to measure the resistance of the metal line. The thermometer was used to measure the temperature of the surface of the sample wafer. Currents of -300 mA, -150 mA, 0, 150 mA, and 300 mA were fed into the Peltier module; the resistance and the temperature of the metal line were measured respectively after the surface temperature of the wafer was completely stable. Figure 3.9 shows the experimental setup. By plotting the temperature corresponding to the five different resistances, the slope dT/dR was deduced. The resistance at room

temperature was the measured resistance when the current input to the Peltier module was 0.

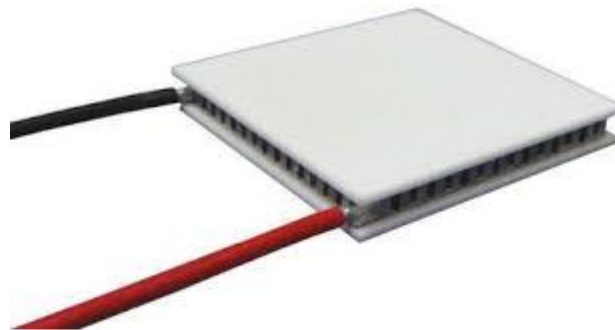

Figure 3.8 Peltier module

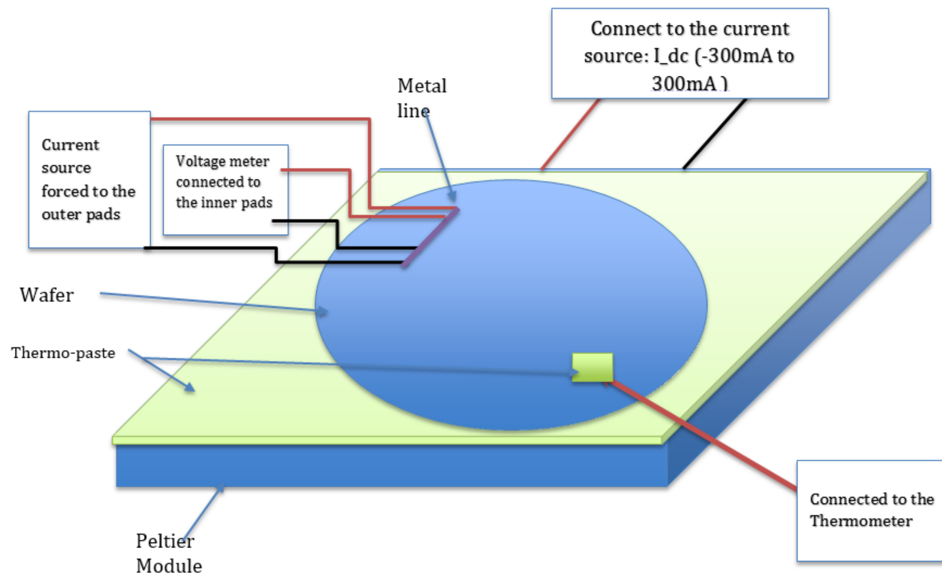

Figure 3.9 Schematic diagram of the TCR measurement setup

3.4 Summary and conclusions

This chapter showed the structures of the three samples we used in this research, their fabrication methods, and the detailed experimental methodology of the 3-omega and 2-omega techniques. Moreover, some essential parameters of the measurement method, such as TCR, were also introduced. All the parameters that were used to extract the anisotropy and thermal conductivity of the superlattice could be measured by the methods shown in this chapter. The analysis of the measured data will be described in the next chapter.

Chapter 4 Data Analysis, Experimental Results, and Discussion

4.1 The purpose of this chapter

This chapter aims to obtain and discuss the thermal conductivities of the materials on the controlled sample and two superlattice wafers (GaAs/AlAs 2/2 nm and 2/8 nm) by analyzing the experimental data obtained from the experiments described in Chapter 3. We will also present the methods used to analyze the experimental data for both the controlled sample and the superlattice samples (e.g., the analytical formula and FEM simulations). More importantly, we will obtain, summarize, and discuss the in-plane and cross-plane thermal conductivities of the 2μm superlattice GaAs/AlAs with 4 nm and 10 nm thickness periods, respectively, as well as the anisotropies of the thermal conductivity. The following paragraph describes the basic analytical method and procedures of this chapter.

The thermal conductivity of the substrate GaAs will be calculated through the equation introduced in Chapter 2 (by analyzing the 3-omega experimental data on the controlled sample). The 50 nm thin film SiO_2 thermal conductivity will be obtained by comparing the 3-omega experimental data and 3-omega FEM simulations of the controlled sample. The discrepancy between the 2-omega experimental data and 2-omega FEM simulation (Fourier's Law) will be analyzed through the controlled sample – this discrepancy will be attributed to the gradual breakdown of Fourier's Law. After obtaining these essential parameters through controlled samples, they will be used in the data analysis of the two superlattice wafers. To analyze the superlattice wafers, we will match the 3-omega experimental data to the 3-omega FEM simulation and match the 2-omega experimental data to the 2-omega FEM simulation simultaneously, as described

in Chapter 2. In the 2-omega matching process, we expect the temperature profile (TP) of the superlattice to be sensitive to the in-plane thermal conductivity, but in the 3-omega matching process, we expect the TP to be more sensitive to the cross-plane thermal conductivity of the superlattice. However, the actual result of matching GaAs/AsAl 2/2 nm and 2/8 nm was different from our expectations and will be described later in this chapter. Moreover, the thermal property of the superlattice of the 3-omega method is sensitive to the thin film SiO_2 thermal property; therefore, the thermal property will be primarily described corresponding to the maximum and minimum of the 50 nm SiO_2 thin film thermal conductivity. Furthermore, the thermal properties and anisotropy between the two superlattice wafers will also be compared.

The essential parameters obtained from the experimental data from both the controlled sample and superlattice wafers will be given in this chapter; more details of the data analysis will be given in the form of tables in Appendix B.

4.2 Controlled sample

The controlled sample has substrate GaAs with 68 nm thin film SiO_2 on top of the substrate. The purpose of the controlled sample is to obtain the thermal conductivities of bulk GaAs: that of thin film SiO_2 and the correction of the Fourier Law (2-omega FEM model), which are required to extract the superlattice thermal conductivity and anisotropy correctly. Given below are the methods used to obtain their thermal conductivities and the results. The discrepancy of the FEM model and the experimental data of the 2-omega method are also described below.

4.2.1 The thermal conductivity of the bulk GaAs

As mentioned in Chapter 2, the thermal conductivity can be calculated by equation 2.20, which is rewritten as equation 4.1 below. V_O is the same as $V_{1\omega}$ in the original equation.

$$k = \frac{P}{2\pi l} * \frac{\ln(\frac{\omega 2}{\omega 1}) * TCR * Vo}{2Vo * \left(V_{3\omega,\omega=\omega 1} - V_{3\omega,\omega=\omega 2}\right)}$$

$$= \frac{\frac{{V_{1\omega}}^2}{Ro}}{2\pi l} * \frac{\ln(\frac{\omega 2}{\omega 1}) * TCR * V_{1\omega}}{2 * \left(V_{3\omega,\omega=\omega 1} - V_{3\omega,\omega=\omega 2}\right)}$$

$$= \frac{TCR}{4\pi l Ro} * \frac{\ln(f2) - \ln(f1)}{\frac{V_{3\omega,\omega=\omega 1} - V_{3\omega,\omega=\omega 2}}{{V_{1\omega}}^3}}$$

$$= \frac{1}{2\pi \log_{10} e} * \frac{\log_{10} f2 - \log_{10} f1}{\frac{2LRo}{TCR} * \frac{V_{3\omega,1} - V_{3\omega,2}}{{V_{1\omega}}^3}} \quad (4.1)$$

The final result of equation 4.1 is what we used to calculate the bulk GaAs; all the parameters in it can be measured. In equation 4.1, e is 2.718, L is the length of the metal line, Ro is the resistance of the metal line, V_O is equivalent to $V_{1\omega}$, and $V_{1\omega}$, $V_{3\omega}$ are measured under the corresponding frequencies. The TCR of the aluminum is approximately 0.00289 on average. Instead of measuring voltages under two frequencies in 4.1, a group of frequencies between 155 Hz and 2000 Hz were used; therefore, the following equation, 4.2, is used to conduct the calculation of the thermal conductivity of GaAs:

$$k = \frac{1}{2\pi \log_{10} e} * \frac{\log_{10} f2 - \log_{10} f1}{\frac{2LRo}{TCR} * \frac{V_{3\omega,1} - V_{3\omega,2}}{V_{1\omega}{}^3}}$$

$$= \frac{1}{2\pi \log_{10} e} * \frac{-1}{\frac{\frac{2LRo}{TCR} * \frac{V_{3\omega,1} - V_{3\omega,2}}{V_{1\omega}{}^3}}{\log_{10} f1 - \log_{10} f2}}$$

$$= \frac{1}{2\pi \log_{10} e} * \frac{-1}{slope} \quad (4.2)$$

$(2LR_O/TCR)*(V_{3\omega}/V_{1\omega}{}^3)$ corresponding to the logarithm frequencies are plotted to form a linear equation; then, the slope of the line (linear equation) is inserted into equation 4.2 to achieve the final result. The results are plotted in figure 4.1 corresponding to the different dimensions of the devices. The averaged thermal conductivity of the bulk GaAs is 55.8 W/m*K, which is very similar to the value given in the literature, 55 W/m*K [34].

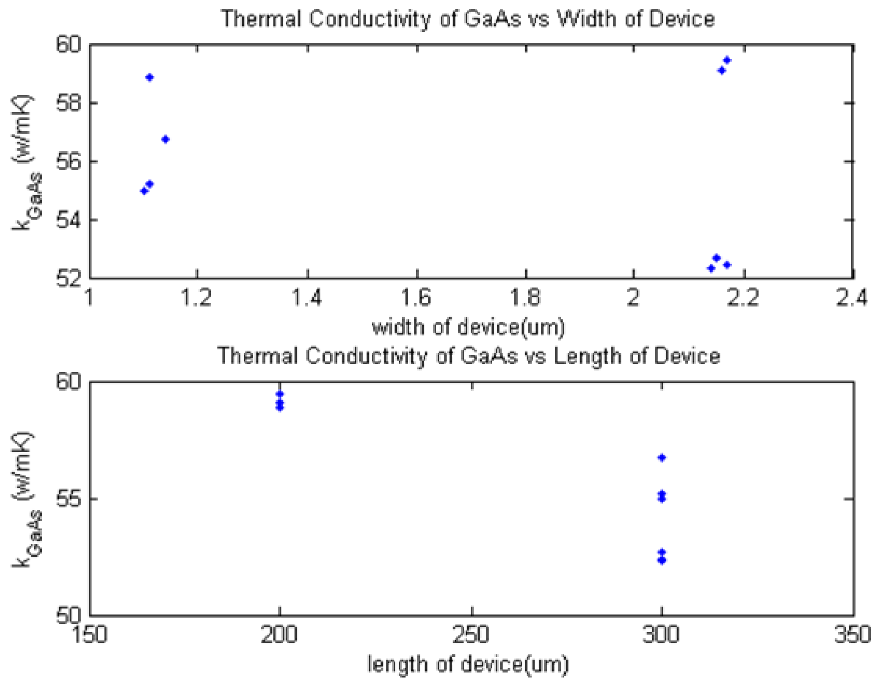

Figure 4.1 The thermal conductivity of GaAs

This result (55W/m*K) proves that the 3-omega method could measure the bulk material accurately and that our measurements of all required parameters leading to this result – such as TCR, Ro, and voltage – are also accurate and reliable. This result is significant in that it directly improves the accuracy and reliability of the data analysis of all the following experimental data. We can see that the dimensions of the metal line (device) do not discernably affect the result. The 300 μm length device shows slightly closer to the 55 W/m*K literature value. We only chose the 300 μm length to conduct the thin film SiO_2 thermal conductivity data analysis for reasons described in the following section.

4.2.2 The thermal conductivity of thin film SiO_2

A. 68 nm thin film SiO_2

A 68 nm thin film SiO_2 is deposited on top of the GaAs substrate of the controlled sample to insulate the electricity between the metal line and the materials under the metal lines. The thin film SiO_2 thermal conductivity on the controlled sample is obtained by comparing the experimental temperature oscillation profile on the surface of the sample to FEM simulation results.

According to equation 2.19 in Chapter 2, temperatures on the surface of the sample, corresponding to the different frequencies (around 155Hz–2000Hz), can be calculated by measuring 3-omega voltage and 1-omega voltage. The equation is then converted to an applied heating power of 1W/cm input power per unit length, which is listed in equation 4.3 below.

$$\Delta T(0) = \frac{\frac{2V_{3\omega}}{V_{1\omega} * TCR}}{\frac{P}{L}} = 2 * L * V_{3\omega} * Ro/({V_{1\omega}}^{3}) \qquad (4.3)$$

where L is the length of the metal line, and R_O is its resistance at room temperature. Because the FEM simulation results are based on a 1 W input heating power and a 1cm long device, the experimental temperature profile should be the same as the FEM simulated temperature profile. We measured 9 devices and matched the simulated temperature profile to the converted experimental temperature profile under 5 to 6 frequencies by adjusting the SiO_2 thermal conductivity and making the GaAs' thermal conductivity fixed at 55.8 W/m*K (measured in our study) in the FEM Model. The matching experimental and FEM results are shown in figure 4.2. The final results of the thin film SiO_2 thermal conductivity are plotted in figure 4.3. More details are listed in Appendix B.

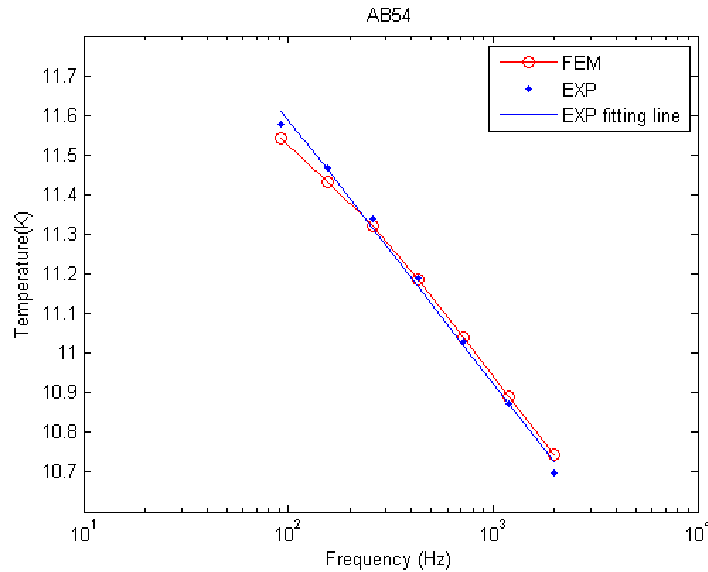

Figure 4.2 Matching example: FEM 3-omega matches the experimental results significantly when choosing proper SiO_2 thermal conductivity; AB54 is the device name that we used to differentiate the devices in our study.

All results of the measured devices are plotted in figure 4.3, but we considered only 300 µm long devices to obtain the final SiO_2 thermal conductivity, because the FEM model is based on the Fourier-series method for the 2D solution of the heat equation under sinusoidal heat-flux excitation, and the heat flux of the 300 µm long metal line is much closer to the 2D heat flux than that of the 200 µm long metal line. From figure 4.3, we can see that the thickness of the metal line does not have an obvious effect on the results. Considering 300 µm long devices, the average thermal conductivity of SiO_2 is 0.574 W/m*K. The range of the thermal conductivity is 0.452 W/m*K to 0.722 W/m*K with a deviation of 0.00115 W/m*K. According to the literature [35, 36, 38, 39], the bulk SiO_2 thermal conductivity is around 1.4 W/m*K, and that of the SiO_2 film is around 1.1 W/m*K. Moreover, some studies show PECVD bulk and thick film SiO_2 to be around 1.1 W/m*K [36]. When the thickness of the dioxide film is below 250 nm, the thermal conductivity of the dioxide decreases as the thickness is reduced [36]. Yamane's study shows that the thermal conductivity of thin film SiO_2 around 60 nm with a 450 °C PECVD process method is around 0.65 W/m*K [36], which is in the range of that in our study. However, according to Burzo's study [38], the existing data of the thermal conductivity of thin film SiO_2 is still different reported from different authors [36–38]. The fabrication process also greatly affects the thermal conductivity of the SiO_2 and the interfacial resistance [38]. Therefore, we could not obtain an accurate literature value to compare it with our study result, and it is critical to use our own experimental results under our own specific fabrication condition summary; the thermal conductivity of the 68 nm thin film SiO_2 has an averaged value of 0.00574 W/m*K and is scattered between 0.00452 W/m*K and 0.00722 W/m*K under our fabrication condition.

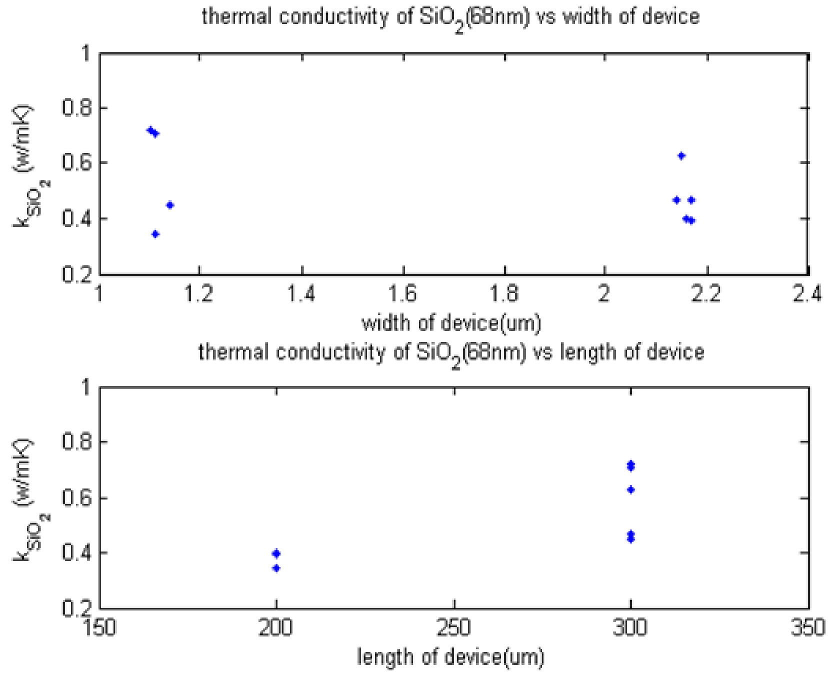

Figure 4.3 Thermal conductivity of thin film SiO_2 vs. dimensions

B. 50 nm thin film SiO_2 in the two superlattice wafers

The actual thickness of the SiO_2 film is 50 nm in the superlattice wafers, which we will study later; thus, the thermal conductivity value of 68 nm SiO_2 should first be converted to that of 50 nm thick dioxide. Considering the contributions from the interface resistance between the metal line and the dioxide film and the interface resistance between the substrate and the dioxide film, the effective thermal conductivity can be expressed by the interface resistance and internal thermal conductivity, as described in equation 4.4 [36].

$$R_f = \frac{d_f}{k_f} = R_i + \frac{d_f}{k_i}, \tag{4.4}$$

where d_f is the thickness of the film, k_f is the observed thermal conductivity of the film or the effective thermal conductivity of the film, R_i is the interface resistance from the metal to the substrate, and k_i is the internal thermal conductivity or the bulk thermal conductivity of the SiO_2. According to Yamane's study, we choose 1.1 W/m*K as the internal PECVD SiO_2 thermal conductivity. The average thermal conductivity of the 50 nm SiO_2 can be obtained by equations 4.5 and 4.6 below, which simply insert related parameters into equation 4.4.

$$\frac{68*10^{-9}m}{0.574} = Ri + \frac{68*10^{-9}m}{1.1} \tag{4.5}$$

$$\frac{50*10^{-9}m}{k_f} = Ri + \frac{50*10^{-9}m}{1.1} \tag{4.6}$$

Therefore, R_i is 5.6*10^-8 Km^2/W, and the average thermal conductivity of 50 nm SiO_2 is 0.49 W/m*K. In Yamane's paper, R_i is 2.9*10^-8 Km^2/W for 450 °C PECVD SiO_2, which is smaller than our value [36]. As we explained before, we will use our own measured data from the specific fabrication process for this study although this conversion procedure might cause further error. The average, minimum, and maximum thermal conductivity of 68nm and 50 nm thin film SiO_2 are summarized in table 4.1 below.

Table 4.1 The thermal conductivity of the thin film SiO_2

The thermal conductivity of the thin film SiO_2		
Samples (unit[W/m*K])	68 nm thickness of the film	50 nm thickness of the film
The averaged value	0.574	0.49
The minimum value	0.452	0.373
The maximum value	0.722	0.643

4.2.3 The discrepancy between the measured 2-omega data and simulated 2-omega analysis data on the controlled sample

As described in Chapter 3, we also conducted 2-omega experiments on the controlled sample to explore the difference in results from the experiment and simulation of the 2-omega method. After the data were collected through the experiment, we converted them into the in-phase temperature profile with 1W/cm input power/unit length (cm) according to equation 4.7 [33].

$$T = \frac{\sqrt{2}L_{cm}V_{2\omega}}{TCR * I_{DC}V_{1\omega}} \quad (4.7)$$

In this equation, L_{cm} is the length of the metal line (all the lengths in the 2-omega method are 300 cm in our study), $V_{2\omega}$ is the second harmonic of the inner pads voltage of the thermometer, $V_{1\omega}$ is the inner pads voltage of the heater, TCR is the temperature coefficient of the resistance of the metal line measured when studying the GaAs thermal conductivity, and I_{DC} is calculated by $(V_{DC} - V_{thermo})/1000$. The method of how to measure V_{DC} and V_{thermo} was described in section 3.2.2. All the parameters have been

measured and determined so that temperature oscillation at the surface under corresponding frequencies can be obtained.

The FEM 2-omega simulations can plot the in-phase temperature profiles under 1W/cm input power/unit length directly after the required parameters are provided. The most basic information includes the dimensions of the device, thermal conductivities, and heat capacities of all the materials. The material information used in this simulation is listed in table 4.2. In the simulations, the thermal conductivity of SiO_2 has no effect on the temperature oscillation; therefore, the scattered values of thin film SiO_2 thermal conductivity have no effect on our 2-omega method and actually improve the accuracy of the simulated results.

Table 4.2 Material parameters in FEM 2-omega simulation

Materials	Thermal conductivity (in-plane) [W/cm*K]	Thermal conductivity (cross-plane) [W/cm*K]	Heat capacity (C_V) [J/K*cm^3]
Metal line (Al/Ti/500 /20 nm)	2.37	2.37[41-43]	2.43 [41–43]
SiO_2 film (68 nm thick)	0.00574 (measured)	0.00574 (measured)	1.93 [41–43]
GaAs substrate	0.00558 (measured)	0.00558 (measured)	1.76 [40]

Three kinds of devices (1 pair of metal lines is a device in the 2-omega method) are investigated, and they have different separations between the two metal lines, whose

edge-to-edge spacings are 0.5 μm, 1 μm, and 2 μm. The real dimensions are used, and the center-to-center spacings are 1080 nm, 1579 nm, and 2575 nm. The temperature oscillations at 2000 Hz of these three kinds of devices are compared and shown in figure 4.4.

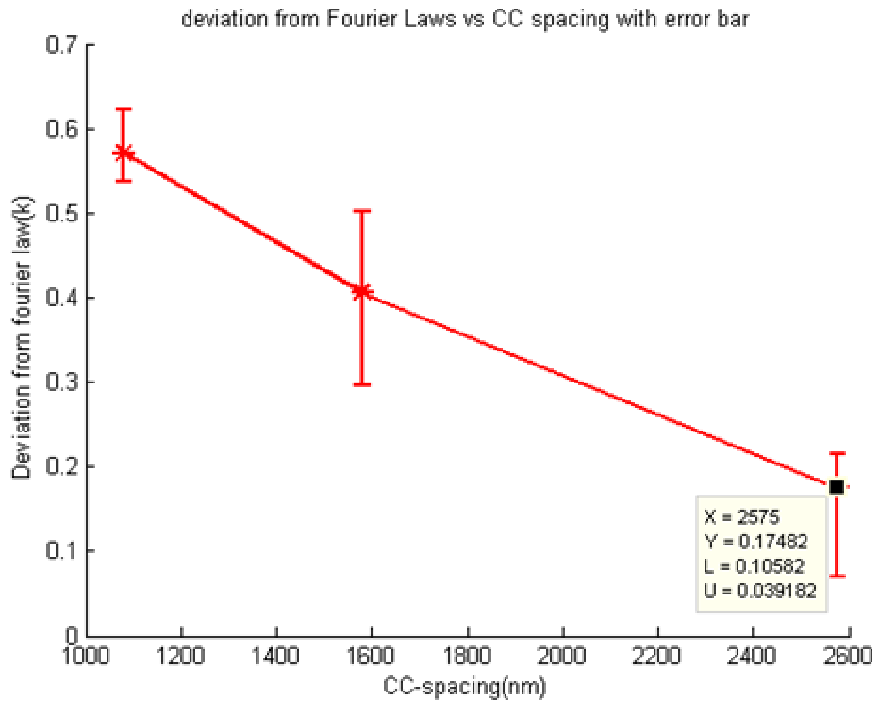

Figure 4.4 The deviation from Fourier Law (FEM 2-omega model). The star indicates the average difference between experiment and FEM corresponding to different CC-spacing. All the experimental values are bigger than the FEM values. The error bar shows the maximum and minimum difference. The solid line aids in reading the figure.

Figure 4.4 shows that the bigger the separation between the two metal lines, the smaller the deviation from Fourier's Law (FEM simulation). Through this experiment on the controlled sample, we found that the 2 μm E-E (2575 nm C-C) spacing has the lowest difference between the FEM and experimental results. Therefore, only 2 μm E-E

separation devices are chosen in the superlattice study. Moreover, figure 4.4 shows that the average deviation is 0.175 K, so it will be added to the FEM 2-omega simulation to correct for this difference and increase the accuracy of the FEM model. This deviation from the Fourier Law result has been explained in terms of the breakdown of the Fourier Law, and details can be found in reference 40.

4.3 Superlattice samples

4.3.1 GaAs/AlAs 2/2 nm superlattice and 2/8 nm superlattice data analysis method

Both 2-omega and 3-omega experiments are conducted on the superlattice wafer to extract the thermal conductivity and the anisotropy of the thermal conductivity. Due to the special structure of the superlattice, the in-plane thermal conductivity k_x and cross-plane thermal conductivity k_z are different. Thus, we define the anisotropy as $\eta = k_x / k_z$. To obtain thermal conductivities in both directions (kx, k_z), the FEM simulations are iteratively matched to the experimental results. The process is done manually, noting that the 2-omega method and 3-omega method are designed to be more sensitive to k_x and k_z, respectively. This idea was introduced in Chapter 2, section 2.3. In practice, however, we found that both the 2-omega and 3-omega methods are more sensitive to k_z than k_x when the superlattice is 2 μm. In the 2 μm superlattice, TO is 5–7 times more sensitive to k_z than to k_x. When reducing both in-plane thermal conductivity and cross-plane thermal conductivity, TO will increase in 3-omega FEM simulations. Meanwhile, we need to increase the in-plane thermal conductivity and decrease the cross-plane to increase TO in the 2-omega FEM simulations. By matching the 3-omega experimental results to FEM 3-omega simulation results and matching the 2-omega experimental results to its simulation results, the anisotropic thermal conductivity of the GaAs/AlAs

2/2 nm superlattice is obtained. To explore the sensitivity to the value of the oxide conductivity deduced through the measurements on the control sample, we conducted 6 pairs of this kind of matching on the GaAs/AlAs 2/2 nm superlattice and 5 pairs on the GaAs/AlAs 2/8 nm corresponding to minimum, maximum, and average SiO_2 thermal conductivity.

As an example, the figure from one pair of the devices/matching is shown in figure 4.5. From figure 4.4, (a) is the 3-omega matching, and the overall fit is good; and (b) is the 2-omega data matching, and the overall matching is excellent. Importantly, after matching the first pair of 2-omega method matching and 3-omega method matching, it is easy for other pairs, since they follow the same rules. The results are detailed in figures 4.6 through 4.9 in the following sections and in the tables in Appendix B.

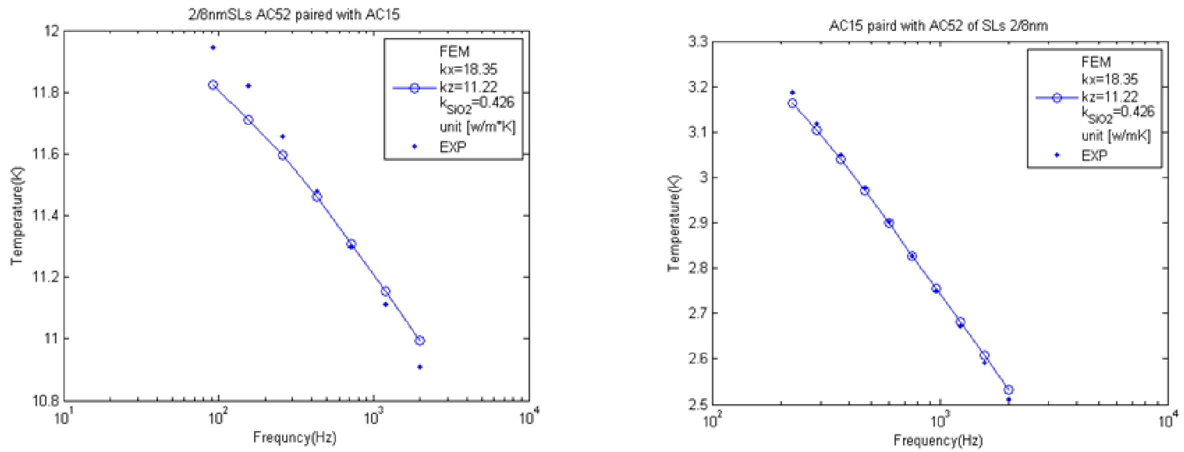

Figure 4.5 (a) Left: 3-omega data matching and (b) Right: 2-omega data matching; the thermal conductivity is a value in the range between 0.373 and 0.643 [W/m*K]. This figure is an example, and all of the matchings in the study are similar to this figure.

4.3.2 The GaAs/AlAs 2/2 nm superlattice results and discussions

The in-plane thermal conductivity of the GaAs/AlAs 2/2 nm superlattice is 7.55 W/m*K, and the cross-plane value is 6.84 W/m*K when choosing average SiO_2 thermal conductivity 0.49 W/m*K. The corresponding anisotropy is 1.13±0.092. Because our results are dependent on the SiO_2 thermal conductivity, the data have been analyzed based on the minimum SiO_2 thermal conductivity 0.373 W/m*K, the average SiO_2 thermal conductivity 0.49 W/m*K, and the maximum SiO_2 thermal conductivity 0.643 W/m*K. Figure 4.6 shows the thermal conductivity of the GaAs/AlAs 2/2 nm superlattice depending on the SiO_2 thermal conductivity; figure 4.7 shows the anisotropy.

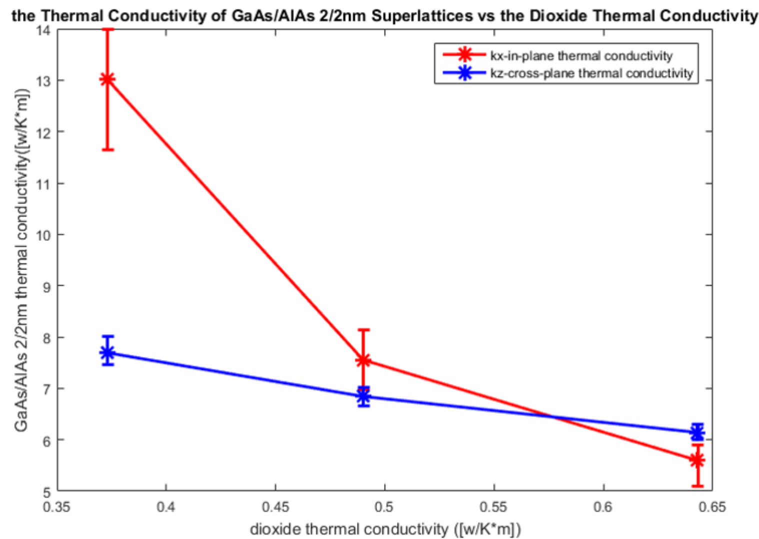

Figure 4.6 The thermal conductivity of the GaAs/AlAs 2/2 nm 2 µm thick superlattice. This is plotted depending on the thermal conductivity of the SiO between its minimum and maximum limits.

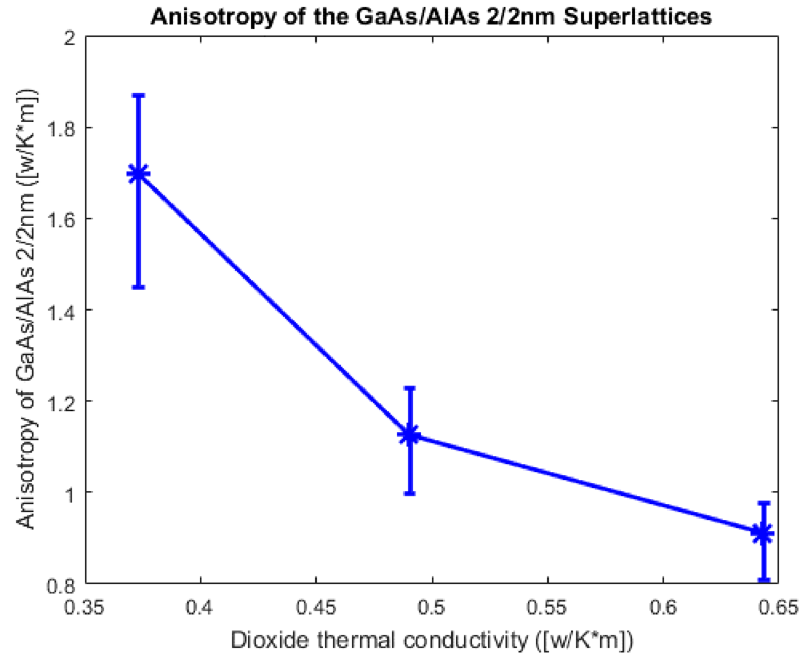

Figure 4.7 Anisotropy of the GaAs/AlAs 2/2 nm 2 µm thick superlattice

The 2-omega data analysis is not sensitive to the SiO_2 thermal conductivity, while the 3-omega data analysis is very sensitive to it. Because both the 2-omega and 3-omega are used to study superlattice anisotropic thermal conductivity in this research, we need to explore the effect of the thermal conductivity on the final results. When SiO_2 thermal conductivity ranges from minimum to maximum value, the cross-plane thermal conductivity of the GaAs/AlAs varies slightly between 6.14 W/m*K and 7.69 W/m*K; in-plane thermal conductivity varies strongly from 5.6W/m*K to 13.02 W/m*K. Additionally, the anisotropy ranges from 0.91 to 1.7. Reports on the GaAs/AlAs 2/2 nm with a 3.5 µm superlattice thickness show that the experimental k_x is around 8.05±0.48 W/m*K, k_z is 6.5±0.5 W/m*K, and anisotropy is 1.2±0.12 [23]. These numbers are very close to our results under the average SiO_2 thermal conductivity. If we could obtain a more consistent dioxide layer thermal property, or if we could design a method that only uses the 2-omega method, our study would be able to give a more reliable result.

Furthermore, the data analysis on the devices with very close real dimensions gives very close results, which proves that our measured data are very stable. Lastly, if we consider all the analyzed devices, the error percentage of the anisotropy under the fixed dioxide thermal conductivity is within 10%.

4.3.3 The GaAs/AlAs 2/8 nm results

In the GaAs/AlAs 2/8 nm 2 μm superlattice sample, the in-plane thermal conductivity of GaAs/AlAs 2/8 nm is 12.91 W/m*K, and the cross-plane thermal conductivity is 10.33 W/m*K, assuming the average SiO_2 thermal conductivity as deduced from control sample 3-omega measurements. The corresponding anisotropy of the sample is 1.25±0.087. The thermal conductivity and anisotropy of this sample are also studied with respect to the thermal conductivity of SiO_2, ranging from 0.373 W/m*K to 0.643 W/m*K, and are plotted in figure 4.8 and figure 4.9. Details are shown in Appendix B.

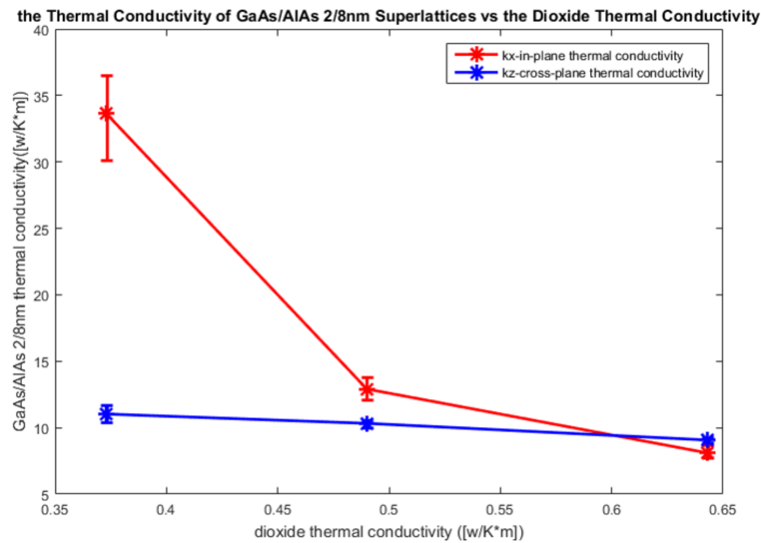

Figure 4.8 Thermal conductivity of GaAs/AlAs 2/8 nm 2 μm thick superlattice

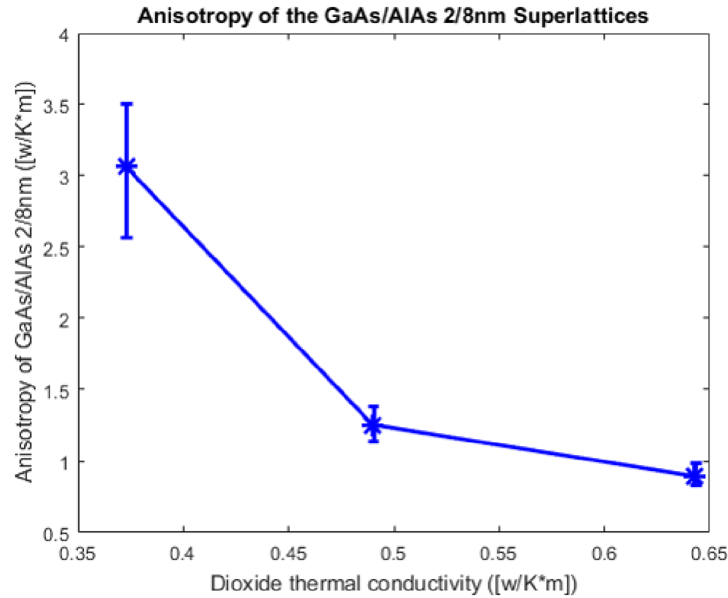

Figure 4.9 Anisotropy of GaAs/AlAs 2/8 nm 2 µm thick superlattice

In figure 4.8 and figure 4.9, the results corresponding to the minimum SiO_2 thermal conductivity are much higher when compared with the average and maximum SiO_2 thermal conductivity. During the process of matching the 2-omega experimental data to the 2-omega simulation data, we found that the FEM 2-omega model is almost not sensitive to the in-plane thermal conductivity of 2 µm thick superlattice when the in-plane k_x is between 22 and 35 W/m*K. This suggests that the results obtained under the lowest dioxide thermal conductivity are not very reliable. If the thermal conductivity varies in a small range, such as from 0.45 to 0.55 W/m*K, the anisotropy ranges from approximately 1.15 to 1.65. So, if we could limit the variations of dioxide thermal conductivity to a smaller range, our final results on the superlattice would be more reliable and consistent.

4.3.4 Comparison of thermal conductivities of GaAs/AlAs from our research with previous results

Figure 4.10 summarizes the results of our research and previous studies on GaAs/AlAs superlattice from different authors. Some researchers concluded that superlattice with higher period thickness has higher thermal conductivities. However, some theoretical predictions report that superlattice has a minimum thermal conductivity at a certain period thickness [28, 29, and 44]. We currently could not show a reliable and clear trend of the thermal conductivities when the period thickness changed, but, in general, both our results and previous results show that the period thickness has a big effect on the thermal conductivities of GaAs/AlAs superlattice.

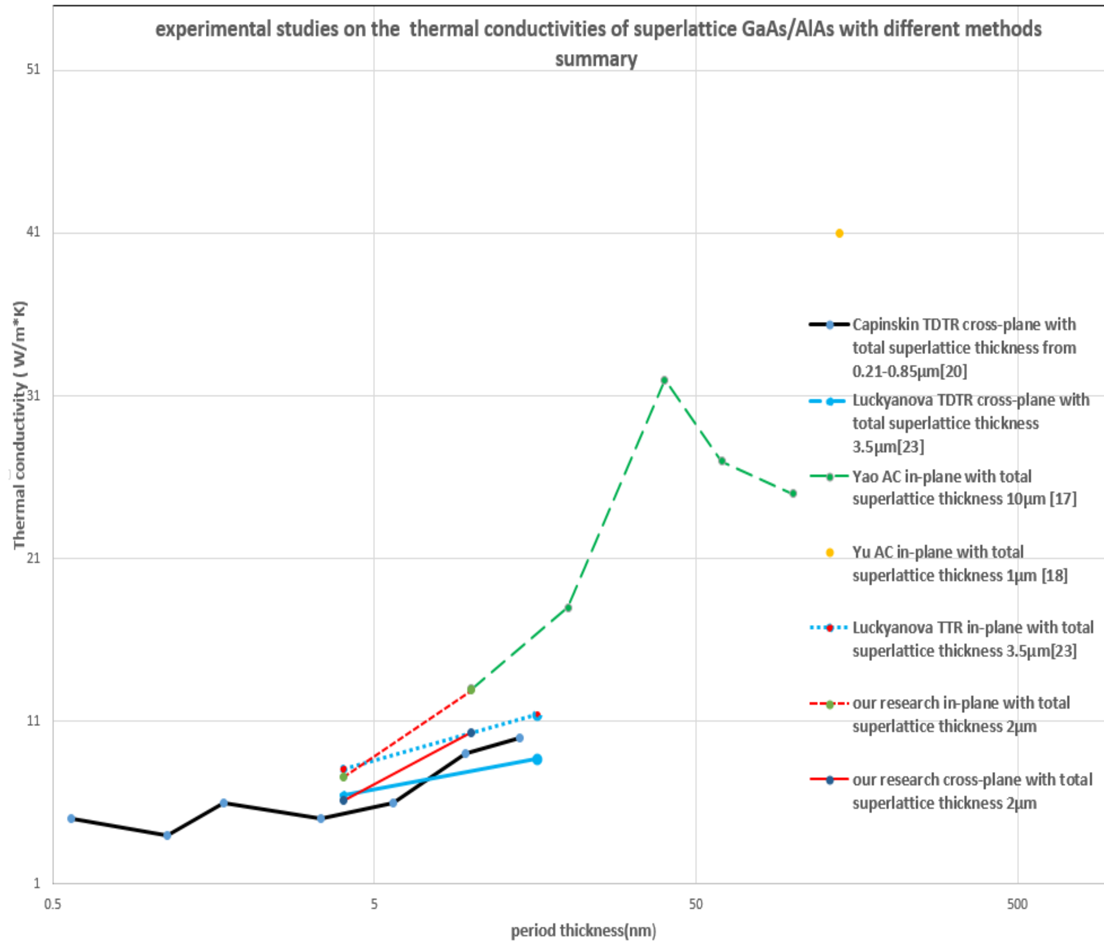

Figure 4.10 Comparisons of thermal conductivities GaAs/AlAs superlattice from different periods, thicknesses, and methods

4.4 Conclusions and summary of this chapter

In this chapter, the methods to analyze the experimental data were described, and the results of the data analysis were shown and discussed. We primarily obtained the parameters below. The correction of 2-D Fourier Law is 0.175 K for 0.5 µm devices (EE spacing 2 µm) in our study. The substrate GaAs is 55.8±2.8 W/m*K and is very close to the literature value of 55 W/m*K. The 68 nm thin film SiO_2 is 0.574±0.115 W/m*K, and the 50 nm thin film SiO_2 is 0.49 W/m*K on average and ranges from

0.373 W/m*K to 0.643 W/m*K. The thermal conductivity of the thin film dioxide is sensitive to the fabrication process (method and temperature), so no exact literature value can be referred to, although the average value is close to some literature reports with the same method. The superlattice thermal conductivity of the FEM 3-omega method is sensitive to the SiO_2, and below, values are reported corresponding to the average SiO_2 thermal conductivity. The GaAs/AlAs 2/2 nm superlattice thermal conductivity is 7.55 W/m*K (in-plane) and 6.14 W/m*K (cross-plane); the anisotropy is 1.13±0.092. The GaAs/AlAs 2/8 nm superlattice thermal conductivity is 12.91 W/m*K (in-plane) and 10.33 W/m*K (out-plane); the anisotropy is 1.25±0.087. These superlattice values are very close to some reports on the same sample done by another research group. Although the anisotropic thermal conductivity of superlattice is affected by some unpredictable elements, such as the inconsistent SiO_2 values, our method works on the 2 µm GaAs/AlAs superlattice in general. In addition, the period thickness should play an essential role in the superlattice thermal conductivities from our research and from previous studies by others.

Chapter 5 Conclusion and Future Work

5.1 Purpose of this chapter

This chapter summarizes the research, results, and challenges met while carrying out the study. Finally, possible future work is suggested.

5.2 Summary of the research/thesis and conclusions

We researched the thermal conductivities of superlattices, primarily because this knowledge has practical applications, such as in thermoelectrics and optoelectronics, and accurate data related to the anisotropic thermal conductivity of superlattices are especially limited. In this research, we studied one controlled sample and two GaAs/AlAs superlattice samples using a combination of the 2-omega and 3-omega techniques. The experimental data are analyzed using the analytical formula and the FEM model.

The controlled sample includes a GaAs substrate and a SiO_2 thin film on top of it; it has two main functions. The first is to extract the thermal conductivities of GaAs and a SiO_2 thin film (68 nm). We primarily use the 3-omega technique to extract the experimental data and the analytical formula as well as the 3-omega FEM model to obtain the bulk GaAs and SiO_2 thermal conductivities separately. The second is to identify the discrepancy between the experimental values and FEM simulation values (based on Fourier's Law) for the 2-omega technique. After obtaining these values, they are used to analyze the superlattice samples or to correct our 2-omega FEM model.

Both the GaAs/AlAs superlattice samples have a 2 μm thick superlattice layer. We designed samples with two different periods: 4 nm (GaAs/AlAs 2 nm/2 nm) and 10

nm (GaAs/AlAs 2 nm/8 nm). Both the 3-omega and 2-omega techniques are sensitive to both in-plane (kx) and cross-plane (k_z) thermal conductivities in our case (2 μm thick film, 2 μm wide metal line in the 3-omega technique and a pair of 2 μm in the 2-omega technique). Finally, we obtained the anisotropic thermal conductivity of superlattices after matching the experimental values to the simulation values by tuning k_x and k_z manually.

In this research, the thermal conductivity of bulk GaAs is 55.8 ± 2.8 W/m*K. The 68 nm SiO_2 thin film is 0.574 ± 0.115 W/m*K, and the 50 nm SiO_2 thin film is 0.49 W/m*K on average, and it ranges from 0.373 W/m*K to 0.643 W/m*K. Although the measured 50 nm thick SiO_2 thermal conductivity varies over a range, the measured average value under our own specific fabrication process is still used, because the fabrication condition has a significant effect on the thermal conductivity of the SiO_2 thin film. Moreover, the correction of the FEM model to account for quasi-ballistic effects is 0.175 K for the 2-omega method with a pair of 0.5 μm metal lines with 2 μm edge-to-edge separation.

The thermal conductivities of the GaAs/AlAs 2/2 nm superlattice are 7.55 W/m*K (in-plane) and 6.14 W/m*K (cross-plane), and the anisotropy is 1.13 ± 0.092. The thermal conductivities of the GaAs/AlAs 2/8 nm superlattice are 12.91 W/m*K (in-plane) and 10.33 W/m*K (out-plane), and the anisotropy is 1.25 ± 0.087. Two results are worth clarifying here. First, the superlattice results are dependent on the measured thermal conductivity of SiO_2, and the data above are deduced using the average thermal conductivity of SiO_2. Second, the thermal conductivities of the GaAs/AlAs 2/8 nm (2 μm total thickness) superlattice in both directions are greater than those of the GaAs/AlAs 2/2 nm (2 μm total thickness) superlattice. Because we have only two

samples, we can only show that the periodic thickness affects the thermal conductivity, but we could not derive specific relations. Some authors have identified relations between period thicknesses and thermal conductivities, but more measured samples and reliable methods are required to provide a reliable conclusion.

5.3 Problems or challenges

Through this research, we found that the combination of the 2-omega and 3-omega techniques could extract the in-plane and cross-plane thermal conductivities of a 2 μm thick GaAs/AlAs superlattice. In addition, the experiments that measure the required parameters in the research are not complex. However, we met some challenges when conducting this research.

First, when we measured the thermal conductivities of the SiO_2 thin film in the controlled sample, the values varied across a small range. As the thermal conductivities of a very thin SiO_2 film are affected by the fabrication process, we could not obtain an accurate literature value to which we could refer. The reason for these small variations is unclear thus far. Another challenge in this research is that the 3-omega technique is sensitive to the thermal conductivity of SiO_2. If the value we obtained from the measured SiO_2 is inaccurate, it will increase the error in our final superlattice thermal conductivity results. Third, the sensitivity of the 2-omega FEM model to in-plane thermal conductivity is affected by the magnitude of the in-plane thermal conductivity itself. For example, when it is in the range of 21–35W/m*K in a 2 μm film, the 2-omega technique is no longer sensitive to the in-plane conductivity. The challenges identified in this research are essential, but they are solvable. We will present in the next section

some possible work we could consider to solve these problems and improve this technique.

5.4 Future work

5.4.1 Measurement of the SiO_2 thin film

The results used in our final calculation are not from a 50 nm SiO_2 thin film directly, because our controlled sample has a 68 nm thick SiO_2 layer. The thickness deviated from the target for unknown reasons during the fabrication process. Therefore, we should measure a SiO_2 film having the exact same thickness as that in the superlattice layer to reduce the error caused by the conversion of the thermal conductivity from different layer thicknesses.

5.4.2 The design of the experiment – a wider metal line in the 3-omega experiment

If we cannot solve the variation in the thermal conductivity of SiO_2, we have other methods to improve our technique. We have witnessed that the thermal conductivity of SiO_2 has no effect on the 2-omega technique. Therefore, as long as we can reduce the effect on the 3-omega technique, we need not worry about the variation in the thermal conductivity of the SiO_2 layer in our superlattice study. From [16], when the metal line width is comparable to the thickness of the measured film, the 3-omega technique is sensitive to both in-plane and cross-plane thermal conductivities; when the metal line width is much wider than the measured film thickness, the 3-omega technique is only sensitive to the cross-plane thermal conductivity. Moreover, we found that the thermal conductivity of SiO_2 had little effect on cross-plane thermal conductivity in our research. Therefore, we can use a much wider metal line than that used in our research (2 µm), such as a 10 µm, 20 µm, or 30 µm wide metal line. This design can not only

eliminate or reduce the effect on the thermal conductivity of SiO_2 but also render our 3-omega technique sensitive only to the cross-plane thermal conductivity of the superlattice.

5.4.3 The data analysis method and check of the simulation results

The data analysis in our controlled sample is easy and clear, so we can continue using these FEM models. However, in the superlattice data analysis, we found that the 2-omega and 3-omega techniques were sensitive to both the in-plane and cross-plane thermal conductivities. This actually increases the time to obtain the anisotropic thermal conductivity, but it will not affect the accuracy of the final results. However, if we can use a computer program to complete the matching process, we do not need to consider whether the 2-omega technique is sensitive to in-plane only or both directions, and it also removes the tedious matching process. The table in the next section is obtained using an optimization program written in MATLAB® [45]. We can optimize the program in the future to improve our technique when researching the thermal properties of superlattices. In addition, when we investigate materials having a high thermal conductivity (such as greater than 20 W/m*K), we might choose to simulate the results using the FEM model or the newly developed matching program prior to the experiments to verify the feasibility of this technique in relation to the specific material.

5.4.4 The anisotropy table for future reference

Table 5.1 below shows the numerical simulation results for future reference [2]. This simulation is designed to explore for what kinds of superlattice our technique works best if the SiO_2 effect still exists. In this simulation, we considered 20 different possible samples, which are five different anisotropic materials paired with four different film thicknesses. Because the experimental results for all 20 samples are

unknown, we assumed the simulated results with $k_x = 10*\eta^{1/2}$, $k_z = 10/\eta^{1/2}$, where η is the anisotropy, under the average SiO_2 thermal conductivity of 0.49 W/m*K as the experimental results. The anisotropy of each sample was obtained through optimization programming with the minimum and maximum SiO_2, respectively.

Table 5.1 Anisotropy Table

"Actual" Anisotropy (k_x/k_z)	The anisotropy range [a, b]: a is obtained under the minimum SiO_2 thermal conductivity (0.373 W/m*K) and b under the maximum value (0.643 W/m*K)			
	SLs =0.5 µm	1 µm	2 µm	10 µm
1.1 (10.48/9.53)	[0.5103,1.6478]	[0.7641, 1.3399]	[0.9364 , 1.1977]	[1.0283, 1.1398]
1.5 (12.25/8.16)	[0.8167, 2.1348]	[1.1086, 1.7637]	[1.3497, 1.6136]	[1.4335, 1.5521]
2.0 (14.14/7.07)	[1.1638 , 2.7217]	[1.5969, 2.2882]	[1.8248, 2.1345]	[1.9140, 2.0679]
4.0 (20/5)	[2.6778 , 4.9288]	[3.5001, 4.3751]	[3.7323, 4.2063]	[3.8384, 4.1245]
10 (31.6/3.16)	[8.3091 , 1.2193]	[9.2153, 10.5932]	[9.4895, 0.4015]	[9.6198, 10.310]

A 10 µm wide metal line was used in the 3-omega model, and a pair of 0.5 µm wide metal lines was used in the 2-omega model. We can see that good results are

achieved in the 2 μm and 10 μm films, especially with greater anisotropy, even considering the full range of measured SiO_2 thermal conductivities.

5.5 Summary

The combination of the 2-omega and 3-omega techniques when studying GaAs/AlAs superlattices works in general. Although challenges arose during our study, improvements to our technology are possible. We expect that this research could assist us in understanding the 2-omega and 3-omega techniques for studying anisotropic superlattice thermal conductivity. The improved techniques and numerical simulations could finally contribute to measuring the thermal conductivities of superlattices accurately and simply, leading to improvements in thermoelectrics and optoelectronics.

References

1. H. Alam and S. Ramakrishna, “A review on the enhancement of figure of merit from bulk to nano-thermoelectric materials,” *Nano Energy*, vol. 2, no. 2, pp. 190–212, 2013.
2. International Energy Agency. *Power Generation from Coal Measuring and Reporting Efficiency Performance and CO2 Emissions*. 2010.
3. G. Chen, M. S. Dresselhaus, G. Dresselhaus, J.-P. Fleurial, and T. Caillat, “Recent developments in thermoelectric materials,” *Int. Mater. Rev.*, vol. 48, no. 1, pp. 45–66, 2003.
4. W. C. Kim, “Thermal transport in nanostructured materials,” *Dissertation of University of Calfornia, Berkeley*, 2005.
5. Fairbanks, "Thermoelectric applications in vehicles status 2008." US Department of Energy, 2008.
6. L. D. Hicks and M. S. Dresselhaus, “Effect of quantum-well structures on the thermoelectric figure of merit,” *Phys. Rev. B* ,vol. 47, no. 19, pp. 12727–12731, 1993.
7. G. Chen and A. Shakouri, “Heat transfer in nanostructures for solid-state energy conversion,” *J. Heat Transfer*, vol. 124, no. 2, p. 242, 2002.
8. J. Piprek, Y. A. Akulova, D. I. Babic, L. A. Coldren, and J. E. Bowers, “Minimum temperature sensitivity of 1.55 μm vertical-cavity lasers at −30 nm gain offset,” *Appl. Phys. Lett.*, vol. 72, no. 15, p. 1814, 1998.
9. Q. Gu, J. S. Smalley, J. Shane, O. Bondarenko, and Y. Fainman, “Temperature effects in metal-clad semiconductor nanolasers,” *Nanophotonics*, vol. 4, no. 1, 2015.

10. A. T. Ramu and J. E. Bowers, “Analysis of the ‘3-Omega’ method for substrates and thick films of anisotropic thermal conductivity,” J. Appl. Phys., vol. 112, no. 4, p. 043516, 2012.
11. A. T. Ramu and J. E. Bowers, “A ‘2-omega’ technique for measuring anisotropy of thermal conductivity,” *Rev. Sci. Instrum.*, vol. 83, no. 12, p. 124903, 2012.
12. D. G. Cahill and R. O. Pohl, “Thermal conductivity of amorphous solids above the plateau,” *Phys. Rev. B*, vol. 35, no. 8, pp. 4067–4073, 1987.
13. S.-M. Lee, D. G. Cahill, and R. Venkatasubramanian, “Thermal conductivity of Si–Ge superlattices,” *Appl. Phys. Lett.*, vol. 70, no. 22, p. 2957, 1997.
14. T. Borca-Tasciuc, W. Liu, J. Liu, T. Zeng, D. W. Song, C. D. Moore, G. Chen, K. L. Wang, M. S. Goorsky, T. Radetic, R. Gronsky, T. Koga, and M. S. Dresselhaus, “Thermal conductivity of symmetrically strained Si/Ge superlattices,” *Superlattices and Microstruct.*, vol. 28, no. 3, pp. 199–206, 2000.
15. W. L. Liu, T. Borca-Tasciuc, G. Chen, J. L. Liu, and K. L. Wang, “Anisotropic thermal conductivity of Ge quantum-dot and symmetrically strained Si/Ge Superlattices,” *J Nanosci. Nanotechnol.* , vol. 1, no. 1, pp. 39–42, Jan. 2001.
16. T. Borca-Tasciuc, A. R. Kumar, and G. Chen, “Data reduction in 3ω method for thin-film thermal conductivity determination,” *Rev. Sci. Instrum.*, vol. 72, no. 4, p. 2139, 2001.
17. T. Yao, “Thermal properties of AlAs/GaAs superlattices,” *Appl. Phys. Lett.*, vol. 51, no. 22, p. 1798, 1987.
18. X. Y. Yu, G. Chen, A. Verma, and J. S. Smith, “Temperature dependence of thermophysical properties of GaAs/AlAs periodic structure,” *Appl. Phys. Lett.*, vol. 67, no. 24, p. 3554, 1995.

19. I. Hatta, Y. Sasuga, R. Kato, and A. Maesono, "Thermal diffusivity measurement of thin films by means of an ac calorimetric method," *Rev. Sci. Instrum*, vol. 56, no. 8, p. 1643, 1985.

20. W. S. Capinski, H. J. Maris, T. Ruf, M. Cardona, K. Ploog, and D. S. Katzer, "Thermal-conductivity measurements of GaAs/AlAs superlattices using a picosecond optical pump-and-probe technique," *Phys. Rev. B*, vol. 59, no. 12, pp. 8105–8113, 1999.

21. W. S. Capinski and H. J. Maris, "Improved apparatus for picosecond pump-and-probe optical measurements," *Rev. Sci. Instrum.*, vol. 67, no. 8, p. 2720, 1996.

22. A.Schmidt, M. Chiesa, X. Chen, and G. Chen, "An optical pump-probe technique for measuring the thermal conductivity of liquids," *Rev. Sci. Instrum.*, vol. 79, no. 6, p. 064902, 2008.

23. M. N. Luckyanova, J. A. Johnson, A. A. Maznev, J. Garg, A. Jandl, M. T. Bulsara, E. A. Fitzgerald, K. A. Nelson, and G. Chen, "Anisotropy of the thermal conductivity in GaAs/AlAs Superlattices," *Nano Lett.*, vol. 13, no. 9, pp. 3973–3977, Nov. 2013.

24. A.A. Maznev, K. A. Nelson, and J. A. Rogers, "Optical heterodyne detection of laser-induced gratings," *Opt. Lett.*, vol. 23, no. 16, p. 1319, 1998.

25. G. D. Goodno, G. Dadusc, and R. J. D. Miller, "Ultrafast heterodyne-detected transient-grating spectroscopy using diffractive optics," *J. Opt. Soc. Am. B*, vol. 15, no. 6, p. 1791, Jan. 1998.

26. J. A. Rogers, A. A. Maznev, M. J. Banet, and K. A. Nelson, "Optical generation and characterization of acoustic waves in thin films: fundamentals and applications," *Annu. Rev. Mater. Sci.*, vol. 30, no. 1, pp. 117–157, 2000.

27. J. A. Johnson, A. A. Maznev, M. T. Bulsara, E. A. Fitzgerald, T. C. Harman, S. Calawa, C. J. Vineis, G. Turner, and K. A. Nelson, “Phase-controlled, heterodyne laser-induced transient grating measurements of thermal transport properties in opaque material,” *J. Appl. Phys.*, vol. 111, no. 2, p. 023503, 2012.
28. K.-H. Lin and A. Strachan, “Thermal transport in SiGe superlattice thin films and nanowires: Effects of specimen and periodic lengths,” *Phys. Rev. B*, vol. 87, no. 11, 2013.
29. J. Garg and G. Chen, “Minimum thermal conductivity in superlattices: A first-principles formalism,” *Phys. Rev. B,* vol. 87, no. 14, 2013.
30. D.G. Cahill, M. Katiyar, and J. R. Abelson, “Thermal conductivity of a -Si:H thin films,” *Phys. Rev. B*, vol. 50, no. 9, pp. 6077–6081, Jan. 1994.
31. T. Tong and A. Majumdar, “Reexamining the 3-omega technique for thin film thermal characterization,” *Rev. Sci. Instrum. ,* vol. 77, no. 10, p. 104902, 2006.
32. A. Delan, M. Rennau, S. Schulz, and T. Gessner, “Thermal conductivity of ultra low-k dielectrics,” *Microelectron. Eng.*, vol. 70, no. 2-4, pp. 280–284, 2003.
33. Weisstein, Eric W. "Modified Bessel differential equation." From MathWorld--A Wolfram Web Resource. Available: http://mathworld.wolfram.com/ModifiedBesselDifferentialEquation.html
34. NSM Archive maintained by the Ioffe Institute, St. Petersburg, Russia
35. D. G. Cahill, “Thermal conductivity measurement from 30 to 750 K: the 3ω method,” *Rev. Sci. Instrum.*, vol. 61, no. 2, p. 802, 1990.
36. T. Yamane, N. Nagai, S.-I. Katayama, and M. Todoki, “Measurement of thermal conductivity of silicon dioxide thin films using a 3ω method,” *J. Appl. Phys.*, vol. 91, no. 12, p. 9772, 2002.

37. S.-M. Lee and D. G. Cahill, “Heat transport in thin dielectric films,” *J. Appl. Phys.* , vol. 81, no. 6, p. 2590, 1997.

38. M. Burzo, P. Komarov, and P. Raad, “Thermal transport properties of gold-covered thin-film silicon dioxide,” *IEEE Trans. Comp. Packag. Technol.*, vol. 26, no. 1, pp. 80–88, 2003.

39. M. Kleiner, S. Kuhn, and W. Weber, “Thermal conductivity measurements of thin silicon dioxide films in integrated circuits,” *IEEE Trans. Electron Devices*, vol. 43, no. 9, pp. 1602–1609, 1996.

40. T. Ramu, N. I. Halaszynski, J. D. Peters, C. D. Meinhart, and J. E. Bowers, “An electrical probe of the phonon mean-free path spectrum,” Available: https://arxiv.org/abs/1602.00381v2

41. C. Y. Ho, R. W. Powell, P. E. Liley, “Thermal conductivity of the elements: A comprehensive review*,” J. of Phys. and Chem. Ref. Data 3*:Suppl. 1, 1974.

42. P. A. Tipler, *Physics for Scientists and Engineers, 4th Ed.*, W. H. Freeman and Company, New York, 1999.

43. L. Filipovic, “Topography simulation of novel processing techniques”, Dissertation, Vienna University of Technology, 2012.

44. M. V. Simkin and G. D. Mahan, “Minimum thermal conductivity of superlattices,” *Phys. Rev. Lett.*, vol. 84, no. 5, pp. 927–930, 2000.

45. Private communication with Dr. Ashok Ramu

Appendix A

The procedures of fabrications are referred to Ashok Ruma, Jon Peter, and Justin Norman in our research group, who fabricated the samples or used the same samples.

(a) On the controlled sample with GaAs substrate:

68 nm SiO_2 was deposited by plasma-enhanced chemical vapor deposition (PECVD) at 248 °C on a clean, double-sided, polished 2-inch diameter unintentionally doped GaAs wafer. The wafer was coated with photoresist NR9-1000 from Futurrex® and spread to a uniform thickness of 1300 nm by spinning at 2000 rpm. After a 135 °C bake for 3 min, it was exposed to UV radiation under a photo-mask for 0.92 sec in a GCA Auto-stepper. A post-develop bake was performed at 100 °C for 2 min, followed by resist development by exposure to developer MF726 from MicroChemicals® for 20 sec. The development was completed with an O2 plasma exposure for 30 sec to de-scum developed areas. A Ti adhesion layer 20 nm thick was deposited on the developed wafer, followed by a 500 nm Al layer, both deposited by electron-beam (e-beam) evaporation. Finally, the metal was lifted off from undeveloped areas using the 1165 stripper from MicroPosit®.

(b) On the superlattice samples:

The samples were grown on a Varian Gen III molecular beam epitaxy (MBE) system. Dimeric arsenic was supplied by a valved cracker source at a beam equivalent pressure of 9.04e-6 Torr. Gallium and aluminum fluxes were calibrated to give growth rates of 2.50 A/s. The samples were grown on native (100) GaAs substrates at 600 °C following a 10 min oxide desorption under As overpressure at 610 °C. Growth was initiated with a 200 nm GaAs buffer followed by the superlattice structures. AlGaAs

layers were grown via a digital alloy. After forming the superlattice structure, the samples experienced the same procedures as those in part (a) to deposit the 50 μm SiO_2 thin film and Ti/Al 20/500 nm thick metal lines.

Appendix B

This appendix lists three tables, which include more details on the results from the controlled sample and two superlattice wafers.

1. Controlled sample details

Table 1. The thermal conductivity of the 68 nm thickness SiO2 film from the controlled sample

Sample Name on the controlled wafer	Real Dimension (measured)			Measured Parameters used in the calculations and FEM simulations		Thermal conductivity of SiO2
	Width(um)	Length(um)	E-E (um)	TCR	K(GaAs)	w/mK
AA22	2.14	300	0.944	2.89e-3	55.8 w/(m*K)	0.470
AB22	2.17	300	0.944			0.470
AA24	1.14	300	0.95			0.452
AA54	1.1	300	0.69			0.722
AB54	1.11	300	0.685			0.707
AB52	2.15	300	0.657			0.625
Thermal conductivity average =0.574 w/(K*m)Thermal conductivity deviation=0.115 w/(k*m) .The thermal conductivity didn't show very obvious consistency , ranging from 0.45 to 0.72 w/(m*k).						

2. GaAs/AlAs 2/2 nm data analysis with average minimum and maximum dioxide thermal conductivity

Table 2. The data analysis of GaAs/AlAs 2/2nm superlattice

Samples	Dimensions (um)			K_SiO2=0.373(min) [w/(m*K)]			K_SiO2=0.643(max) [w/(m*K)]			K_SiO2=0.49(avg) [w/(m*K)]		
	width	E-E	width	Kx	Kz	**Kx/kz**	Kx	Kz	**Kx/kz**	Kx	Kz	Kx/kz
CC15	0.499	2.12	0.463	11.65	8.02	**1.45**	5.1	6.3	**0.8**	6.99	7.02	**1**
BD15	0.522	2.05	0.563	11.85	8	**1.48**	5.23	6.27	**0.83**	7.09	7.0	**1.01**
BA15	0.586	1.98	0.579	13.35	7.6	**1.76**	5.7	6.12	**0.93**	7.74	6.77	**1.14**
BC15	0.564	2	0.59	13.30	7.58	**1.76**	5.75	6.11	**0.94**	7.8	6.75	**1.16**
CA15	0.584	2	0.580	13.95	7.48	**1.87**	5.9	6.02	**0.98**	8.15	6.67	**1.22**
BB15	0.567	2.02	0.581	13.99	7.47	**1.87**	5.9	6.02	**0.98**	8.2	6.66	**1.23**
Summary: **Note:paried with CA52 (300um*2um)**		**Kx_avg=13.02** **Kz_avg=7.69** **Kx/kz_avg=1.7** **Dev_kx/kz=0.17**					**Kx=5.6** **Kz=6.14** **Kx/kz=0.91** **Dev_kx/kz=0.068**			**Kx=7.55** **Kz=6.84** **Kx/kz=1.13** **Dev_kx/kz=0.092**		

3. GaAs/AlAs 2/8 nm data analysis with average minimum and maximum dioxide thermal conductivity

Table 3. The data analysis of GaAs/AlAs 2/8 nm superlattice

Samples	Dimensions[um]			K_SiO2=0.373(min) [w/(m*K)]			K_SiO2=0.49(avg) [w/(m*K)]			K_SiO2=0.643(max) [w/(m*K)]		
	width	E-E	width	Kx	Kz	Kx/kz				Kx	Kz	Kx/kz
BB15	0.516	2.05	0.509	30.1	11.70	2.57	12.1	10.57	1.14	7.75	9.25	0.84
AC15	0.531	2.05	0.545	32.1	11.3	2.84	12.45	10.5	1.19	7.75	9.16	0.85
BD15	0.472	2.1	0.49	34.4	10.94	3.14	12.9	10.34	1.25	8.1	9.09	0.89
BA15	0.522	2.03	0.545	35.10	10.8	3.25	13.25	10.23	1.3	8.15	9	0.91
CA15	0.476	2.1	0.467	36.5	10.4	3.51	13.85	9.99	1.39	8.75	8.85	0.99
Summary: **Note : paired with AC52 of 3-omega test**		**Kx_avg=33.64** **Kz_avg=11.03** **Kx/Kz=3.06**					**Kx_avg=12.91** **Kz_avg=10.33** **Kx/Kz=1.25** **Dev_kx/kz=0.087**			**Kx=8.1** **Kz=9.07** **Kx/Kz=0.89** **Dev_Kx/Kz=0.054**		